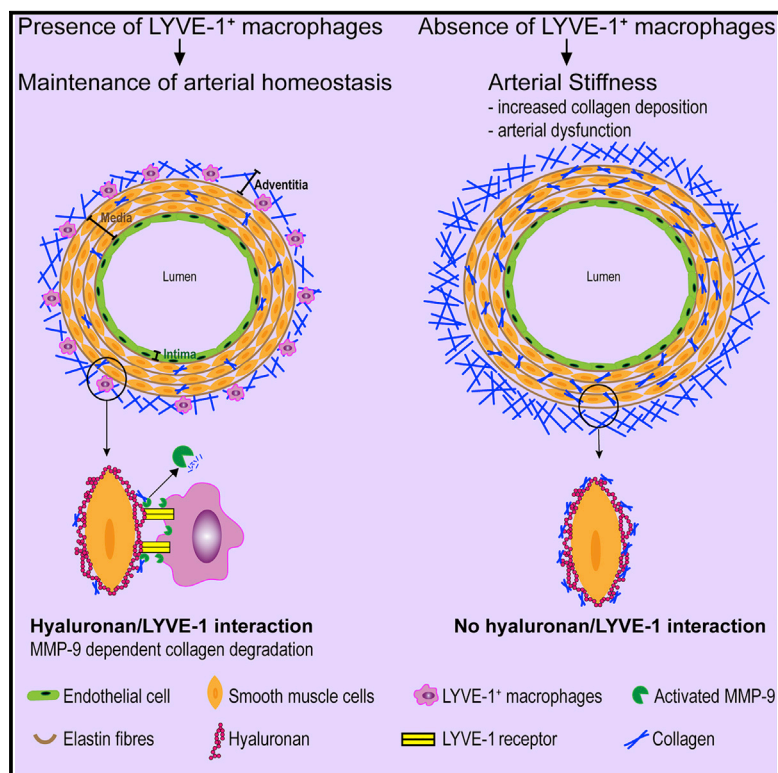


Immunity

Hyaluronan Receptor LYVE-1-Expressing Macrophages Maintain Arterial Tone through Hyaluronan-Mediated Regulation of Smooth Muscle Cell Collagen

Graphical Abstract



Authors

Hwee Ying Lim, Sheau Yng Lim, Chek Kun Tan, ..., David G. Jackson, Florent Ginhoux, Véronique Angeli

Correspondence

micva@nus.edu.sg

In Brief

Macrophages are essential to maintain tissue homeostasis. Lim and colleagues demonstrate that perivascular LYVE-1-expressing macrophages prevent arterial stiffness by controlling the expression of collagen in vascular smooth muscle cells, a process dependent on the engagement of LYVE-1 with hyaluronan on smooth muscle cells.

Highlights

- LYVE-1⁺ macrophages coat murine and human blood vessels harboring smooth muscle cells
- Deficiency in LYVE-1⁺ macrophages induces arterial stiffness and collagen deposition
- LYVE-1⁺ macrophages degrade collagen on smooth muscle cells via pericellular MMP-9
- LYVE-1 on macrophage engages HA on smooth muscle for collagen degradation



Hyaluronan Receptor LYVE-1-Expressing Macrophages Maintain Arterial Tone through Hyaluronan-Mediated Regulation of Smooth Muscle Cell Collagen

Hwee Ying Lim,^{1,12} Sheau Yng Lim,^{1,12} Chek Kun Tan,² Chung Hwee Thiam,¹ Chi Ching Goh,³ Daniel Carbajo,³ Samantha Hui Shang Chew,¹ Peter See,³ Svetoslav Chakarov,³ Xiao Nong Wang,⁴ Li Hui Lim,¹ Louise A. Johnson,⁵ Josephine Lum,³ Chui Yee Fong,⁶ Ariff Bongso,⁶ Arijit Biswas,⁶ Chern Goh,¹ Maximilien Evrard,³ Kim Pin Yeo,¹ Ranu Basu,⁷ Jun Kit Wang,⁸ Yingrou Tan,³ Rohit Jain,⁹ Shweta Tikoo,⁹ Cleo Choong,⁸ Wolfgang Weninger,⁹ Michael Poidinger,³ Richard E. Stanley,⁷ Matthew Collin,⁴ Nguan Soon Tan,^{2,10,11} Lai Guan Ng,³ David G. Jackson,⁵ Florent Ginhoux,³ and Véronique Angeli^{1,13,*}

¹Department of Microbiology & Immunology, Immunology Programme, Life Science Institute, Yong Loo Lin School of Medicine, National University of Singapore, Singapore 117597, Singapore

²School of Biological Sciences, Nanyang Technological University, Nanyang, Singapore 637551, Singapore

³Singapore Immunology Network, A*STAR, Singapore 138648, Singapore

⁴Institute of Cellular Medicine, Newcastle University, Newcastle NE2 4HH, UK

⁵MRC Human Immunology Unit, Weatherall Institute of Molecular Medicine, University of Oxford, John Radcliff Hospital, Oxford OX3 9DS, UK

⁶Department of Obstetrics and Gynaecology, Yong Loo Lin School of Medicine, National University Health System, National University of Singapore, Singapore 119074, Singapore

⁷Department of Development and Molecular Biology, Albert Einstein College of Medicine, New York, NY 10461, USA

⁸School of Material Science and Engineering, Nanyang Technological University, Singapore 639977, Singapore

⁹The Centenary Institute, Newtown, NSW 2050, Australia

¹⁰Institute of Molecular and Cell Biology, A*STAR, Singapore 138673, Singapore

¹¹KK Women's and Children Hospital, Singapore 229899, Singapore

¹²These authors contributed equally

¹³Lead Contact

*Correspondence: micva@nus.edu.sg

<https://doi.org/10.1016/j.immuni.2018.06.008>

SUMMARY

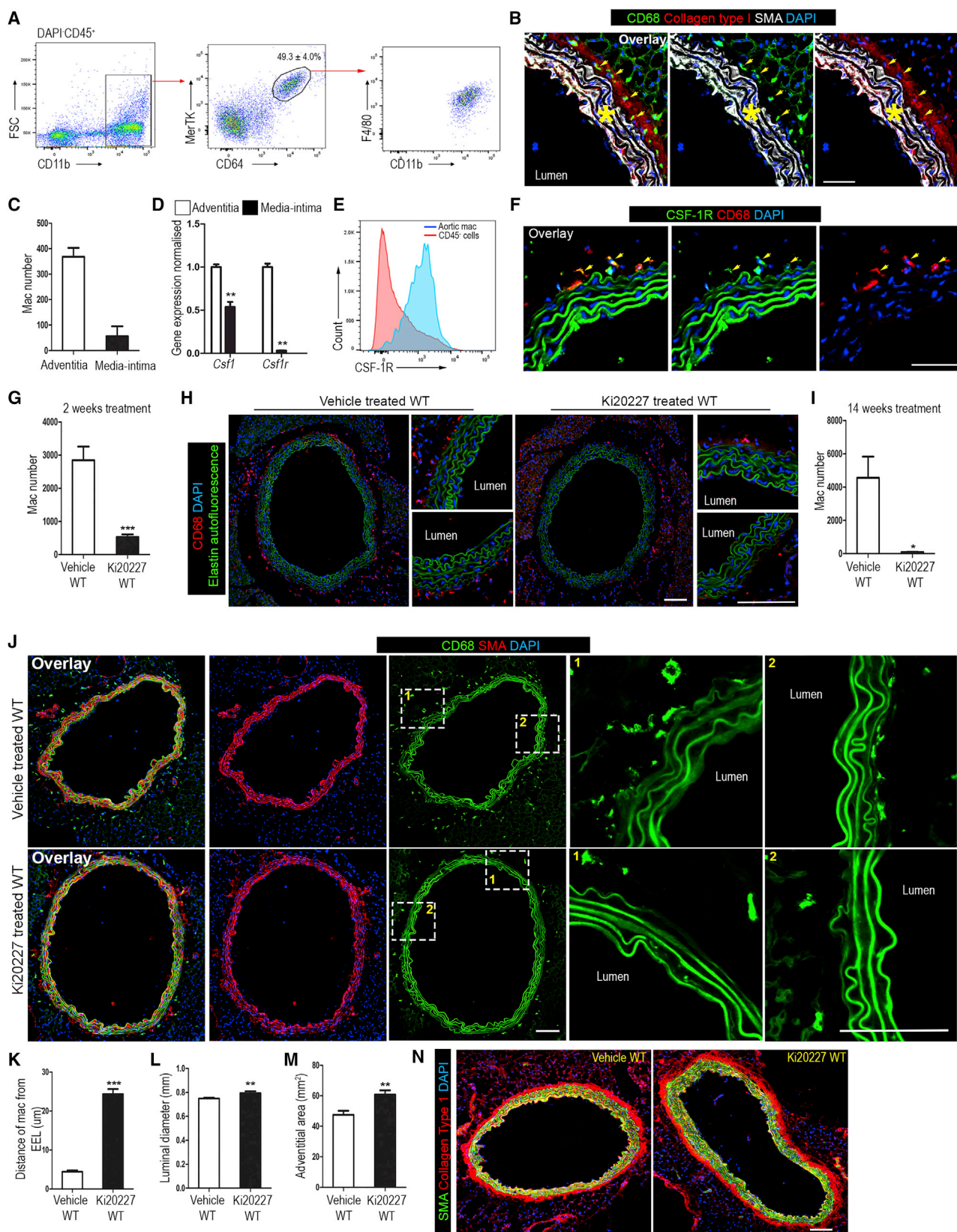
The maintenance of appropriate arterial tone is critically important for normal physiological arterial function. However, the cellular and molecular mechanisms remain poorly defined. Here, we have shown that in the mouse aorta, resident macrophages prevented arterial stiffness and collagen deposition in the steady state. Using phenotyping, transcriptional profiling, and targeted deletion of *Csf1r*, we have demonstrated that these macrophages—which are a feature of blood vessels invested with smooth muscle cells (SMCs) in both mouse and human tissues—expressed the hyaluronan (HA) receptor LYVE-1. Furthermore, we have shown they possessed the unique ability to modulate collagen expression in SMCs by matrix metalloproteinase MMP-9-dependent proteolysis through engagement of LYVE-1 with the HA pericellular matrix of SMCs. Our study has unveiled a hitherto unknown homeostatic contribution of arterial LYVE-1⁺ macrophages through the control of collagen production by SMCs and has identified a function of LYVE-1 in leukocytes.

INTRODUCTION

As part of the circulatory system, arteries function to actively transport oxygenated blood, nutrients, and cells throughout the body in a process that is indispensable for maintaining functional tissue homeostasis. Each artery is composed of three major compartments: the inner intima formed by a single layer of endothelial cells and a fine basement membrane; the media that consists of smooth muscle cell (SMC) layers separated by elastic sheets; and the outer adventitial layer that is composed predominantly of connective tissue, mainly collagen fibers and fibroblasts (Wagenseil and Mecham, 2009). The extracellular matrix (ECM) within the microstructure of large- and medium-sized elastic arteries such as the aorta that is made up of elastin and collagen imparts the elastic properties and strength of the aorta, respectively, and determines efficient blood flow (Kohn et al., 2015).

Changes in the amounts and/or architecture of elastin and collagen in the arterial wall have been shown to affect arterial mechanical function (Kohn et al., 2015). Elastin-haploinsufficient and collagenase-resistant mice have been shown to endure arterial mechanical dysfunction and increased vascular wall rigidity (Vafaie et al., 2014; Wagenseil et al., 2005). In humans, considerable clinical evidence has clearly implicated arterial ECM remodelling in the pathogenesis of the most common forms of aortic diseases associated with aberrant arterial biomechanics such as aging-induced arterial stiffening,





(legend on next page)

atherosclerosis, aneurysms, and dissections (Tsamis et al., 2013). Remodelling of ECM associated with these pathological conditions often results from the imbalance between production and degradation of collagen and elastin in the arterial wall. Increased ECM synthesis by vascular SMCs and adventitial fibroblasts is mediated by fibrotic factors whereas matrix metalloproteinases (MMPs) and tissue inhibitors of MMPs are involved in the degradation of ECM proteins and its control, respectively (Castro et al., 2011; Wagenseil and Mecham, 2009). While regulators of ECM synthesis and degradation in aortic diseases have been well studied, little is known about mechanisms that might limit aberrant ECM production and maintain normal aortic tissue elasticity, strength, and function in normal physiological conditions.

Tissue-resident macrophages are now recognized to fulfil functions beyond those of conventional immune regulation and to play important roles in support of tissue homeostasis. These latter functions of macrophages are highly dependent on the tissue in which they reside and on changes in their environment to which they respond rapidly (Ginhoux and Jung, 2014; Varol et al., 2015). The existence of normal arterial-resident macrophage populations defined by their expression of either conventional or more selective lineage markers has been reported previously (Ensan et al., 2016; Galkina et al., 2006; Jongstra-Bilen et al., 2006). Using a gene profiling approach, Ensan et al. (2016) report a unique gene signature for resident arterial macrophages when compared to other tissue macrophages during adult murine homeostasis. In this report the resident arterial macrophages are replaced by inflammatory infiltrating macrophages upon bacterial infection and returned rapidly to homeostasis when the infection subsides. Although these studies provide important insights into the origin and maintenance of arterial macrophages, they fail to explore their physiological function. Whether arterial macrophages regulate arterial homeostasis is still an open question, in part because functional studies to elucidate their role have focused instead on the formation, damage, or repair of blood vessels during developmental and pathogenic processes (Fung and Helisch, 2012; Simons and Eichmann, 2015; Swirski et al., 2016).

Motivated by the dramatic increase in the current understanding of tissue macrophage homeostatic function, we therefore sought to elucidate whether arterial-resident macrophages

contribute to adult vessel integrity. Our current study focused on murine aorta because this is the largest artery draining directly from the heart to distribute oxygenated blood through the body and its damage results in life-threatening cardiovascular diseases (Kohn et al., 2015). Our results show that aortic-resident macrophages are essential for the maintenance of arterial vessel homeostasis through the regulation of mural cell collagen production. Furthermore, our studies reveal that these functions are carried out by a specialized population of arterial macrophages that interact with the extracellular matrix glycosaminoglycan hyaluronan (HA) in vascular SMCs via the lymphatic receptor LYVE-1.

RESULTS

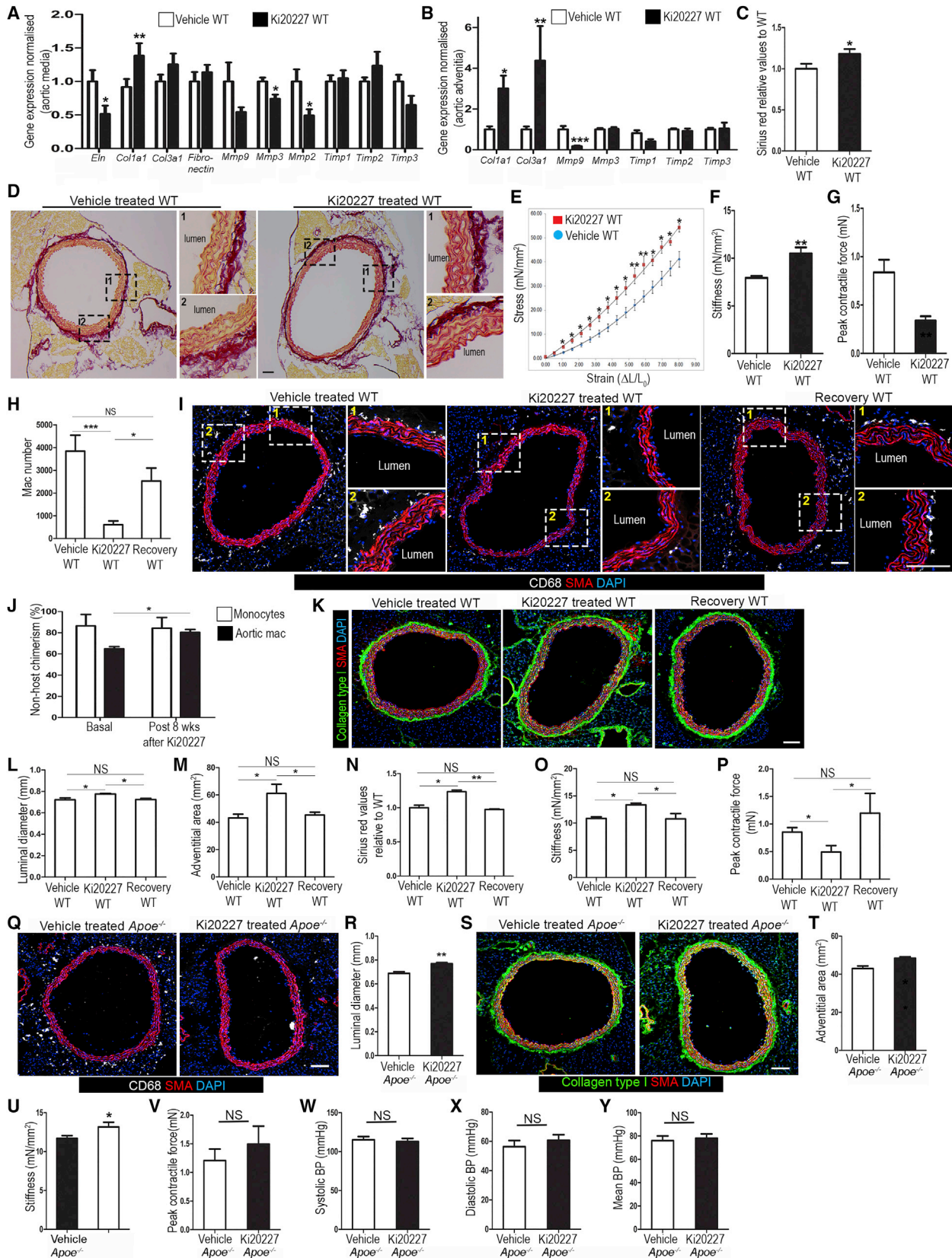
Maintenance of Arterial Macrophages Depends on CSF-1R Signaling in Normal Aorta

We first used flow cytometry and fluorescent microscopy to identify macrophages residing in adult murine aorta under steady-state conditions. We utilized MerTK and Fc γ R1 (CD64) as tissue-resident macrophage markers (Gautier et al., 2012) in our single aortic cell suspension flow cytometry-based analysis. These analyses revealed that MerTK⁺CD64⁺ aortic macrophages in adult wild-type (WT) mice were also F4/80⁺CD11b⁺ (Figure 1A). Immunofluorescence analysis of aortic sections showed that CD68⁺ macrophages mainly resided within the collagen type I (Col I)-rich adventitia in close contact with the medial layer but not within the media and only a few macrophages were occasionally detected in the luminal side of the intima (Figure 1B and data not shown). Further examination of the spatial distribution of macrophages within the arterial wall layers by flow cytometry confirmed that macrophage numbers were markedly higher in the adventitia than in the intima and media (Figure 1C), consistent with the study by Ensan et al. (2016).

To evaluate the contribution of arterial macrophages to vessel homeostasis *in vivo*, we generated a mouse model in which these macrophages are depleted. The macrophage colony stimulating factor (M-CSF) or CSF-1 is critical for the survival, proliferation, and differentiation of tissue macrophages through the activation of CSF-1 receptor (CSF-1R) (Hume and MacDonald, 2012). *Csf1* mRNA was expressed in both the adventitial and medial layers but in higher amounts in adventitia (Figure 1D). In

Figure 1. Depletion of Aortic-Resident Macrophages Leads to Arterial Wall Remodelling

- (A) Gating strategy of macrophages (mean \pm SEM, n = 6).
 (B) Aortic sections stained for Col I, SMA (smooth muscle actin), and CD68 (arrows). Asterisk denotes SMA⁺ media.
 (C) Aortic macrophages number by flow cytometry (mean \pm SEM, n = 2).
 (D) Normalized gene expression of *Csf1* and *Csf1r* in WT aorta (mean \pm SEM; n = 5 per group).
 (E) Flow cytometry analysis of CSF-1R expression by aortic macrophages.
 (F) Aortic sections of MaFIA mice showing CSF-1R expression on adventitial macrophages (arrows).
 (G and H) WT mice received Ki20227 for 2 weeks.
 (G) Aortic macrophages number determined by flow cytometry (mean \pm SEM; n = 13 per group).
 (H) CD68⁺ macrophages in aortic sections.
 (I–N) Analysis of descending aortas from WT mice treated with Ki20227 or vehicle for 14 weeks.
 (I) Aortic macrophage number (mean \pm SEM; n = 4 per group).
 (J) Representative image of aortic sections immunostained for CD68 and SMA. Media elastic lamella is auto-fluorescent (green). Inserts show high magnification.
 (K–M) Distance of CD68⁺ macrophages from external elastin lamella (EEL) (K), luminal diameter (L), and adventitial area (M) (mean \pm SEM; n = 7–9 per group).
 (N) Immunostaining for Col I and SMA.
 Data are collected from 2–3 independent experiments. *p < 0.05**; p < 0.005; ***p < 0.0005. Scale bar = 100 μ m except (B) and (F) = 50 μ m. See also Figure S1.



(legend on next page)

contrast, *Csf1r* was detected only in adventitia where the majority of macrophages reside and the presence of CSF-1R on the surface of aortic macrophages was subsequently confirmed by flow cytometry (Figure 1E). Experiments with Fas-induced apoptosis (MaFIA) transgenic mice that express green fluorescent protein (EGFP) under the *Csf1r* promoter (Burnett et al., 2004) revealed a CD68 and GFP dual-positive macrophage population in aortic sections (Figure 1F). These findings indicated that arterial macrophages may also depend on CSF-1R signaling for their maintenance, and therefore we evaluated the effects of CSF-1R inhibition on aortic macrophages in the steady state. Treatment for 2 weeks with the selective CSF-1R tyrosine kinase inhibitor Ki20227 (Kubota et al., 2009) resulted in a profound depletion of macrophages in aorta of WT mice (Figures 1G and 1H). These findings validate the pharmacological inhibition of CSF-1R signaling as an effective means of depleting aortic macrophages *in vivo*.

Resident Arterial Macrophages Maintain Normal Vascular Wall Structure

We next evaluated the effect of ablating aortic macrophages in the vascular wall. Ki20227 treatment for 14 weeks in WT mice markedly depleted aortic macrophages (Figures 1I and 1J), and the few that remained in the adventitia (Figures 1I and 1J) were no longer in close contact with the medial layer but were instead located predominantly at the outer border of the adventitial layer (Figures 1J and 1K). Notably, monocyte numbers in blood and aortas remained unaffected, showing that Ki20227 treatment did not affect this population (Figures S1A and S1B). The depletion of aortic macrophages in Ki20227-treated animals resulted in partial straightening of elastin fibers and significant vessel dilatation (Figures 1J–1L). Besides changes in the medial wall, significant adventitial thickening was also observed in Ki20227-treated WT aortas (Figures 1M and 1N). Similar results were obtained in the aortas of MaFIA mice following administration of the drug AP20187 to induce Fas-mediated apoptosis in CSF-1R-expressing cells including aortic macrophages (Figures S1C–S1F). Hence the loss of aortic-resident macrophages in the steady state is associated with arterial structural changes.

Resident Arterial Macrophages Control Vascular ECM Environment and Physiological Function

Since elasticity and strength in the normal aorta is governed by the ECM proteins collagen and elastin, we hypothesized that arterial macrophages maintain vascular wall integrity by regulating ECM protein expression. We analyzed the expression of ECM-related genes in aortas from Ki20227-treated WT mice. We found that tropo-elastin (*Elm*), the precursor of elastin, was downregulated in the media of Ki20227-treated WT mice whereas pro-collagen type 1 alpha 1 (*Col1a1*) was markedly upregulated (Figure 2A). The expression of collagen-degrading matrix metalloproteinases *Mmp2* and *Mmp3* were also decreased. In contrast, other pro-collagen forms, MMP inhibitors (TIMPs), and fibronectin were unaffected in the media of Ki20227-treated WT mice. *Elm* was also downregulated in the media of MaFIA mouse aortas following macrophage depletion (Figure S1G). ECM changes in the media of Ki20227-treated WT aortas were accompanied by significantly increased expression of *Col1a1* and *Col3a1* and decreased expression of *Mmp9* in the adventitia (Figure 2B). In support of our gene expression analyses, quantification of total collagen protein using Sirius red immunohistochemistry revealed a significantly increased collagen content in Ki20227-treated WT aortas (Figure 2C). Enhanced collagen deposition was also apparent in the media layer of Ki20227-treated WT aortas (Figure 2D).

Structural modifications of ECM in the arterial wall have been reported previously to alter aortic mechanical function and to impede blood flow (Kohn et al., 2015). To determine the consequences of the structural alterations observed in macrophage-depleted aortas for the passive mechanical properties of the aortic wall, we performed circumferential tensile assays to assess stress-strain relationship in the vessels. Ki20227-treated WT mice displayed increased aortic wall stiffness compared to the vehicle-treated WT group (Figures 2E and 2F), indicating that Ki20227-treated aortas had significantly reduced passive mechanical function. Moreover, the contractile function of the aortas in Ki20227-treated WT mice was compromised, as shown by a significant reduction in the maximal contractile force of aortic rings generated in response to potassium chloride (Figure 2G). However, these mechanical and functional alterations

Figure 2. Resident Macrophages Regulate Vessel Function and ECM Content

(A–G) Analysis of descending aortas from mice treated with Ki20227 or vehicle for 14 weeks. (A and B) Relative gene expression in media and intima (A) and adventitia (B) with $n = 5–10$ per group (mean \pm SEM). (C) Quantification of aorta collagen content by Sirius red (mean \pm SEM, $n = 6–7$). (D) Sirius red-stained aortic sections. (E–G) Biomechanical properties of aortas using circumferential tensile and contractility tests. Stress-strain curve (E), stiffness (F), and maximal contractile force (G) in response to KCl stimulus (mean \pm SEM with $n = 5–7$ mice). (H–P) WT mice received vehicle or Ki20227 for 24 weeks. Recovery WT mice received Ki20227 for the first 14 weeks to induce arterial remodeling and then switched to vehicle for another 10 weeks. (H) Aortic macrophage number (mean \pm SEM; $n = 7–8$ per group). (I) Aortic sections immunostained for CD68 and SMA. Inserts show high magnification. (J) Engraftment of aortic CD45.1⁺ BM cells in irradiated CD45.2 recipients assessed by flow cytometry (mean \pm SEM; $n = 3–4$ per group). (K) Immunostaining for Col I and SMA. (L and M) Luminal diameter (L) and adventitial area (M) (mean \pm SEM; $n = 5–6$ per group). (N) Quantification of aorta collagen content by Sirius red (mean \pm SEM, $n = 6–7$ per group). (O and P) Aortic stiffness (O) and maximal contractile force (P) in response to KCl stimulus (mean \pm SEM, $n = 6–11$ per group). (Q–Y) *Apoe*^{-/-} mice at 9–10 weeks of age received Ki20227 or vehicle for 9 weeks. Descending aorta sections stained for CD68 in (Q) and Col I in (S) with SMA and DAPI co-stain. Luminal diameter (R) and adventitial area (T) (mean \pm SEM; $n = 4–7$ per group). Aortic stiffness (U) and maximal contractile force (V) in response to KCl stimulus (mean \pm SEM, $n = 8–10$ per group). Systolic (W), diastolic (X), and mean (Y) blood pressure (mean \pm SEM, $n = 5–6$ per group). Data are pooled from 2–3 independent experiments. * $p < 0.05$; ** $p < 0.005$; *** $p < 0.0005$. Scale bar = 100 μ m. See also Figure S1.

were not associated with changes in systemic blood pressure (Figures S1H–S1J). We could rule out any direct effects of Ki20227 treatment on SMCs in the aortas, as these express neither *Csf1r* mRNA nor protein (Figures 1D and 1F).

We investigated the possibility that arterial macrophages might have repopulated the adventitia after the cessation of Ki20227 treatment and hence were able to reverse the defects seen in the arterial wall (Figure S1K). We found that arterial macrophage numbers were significantly increased 10 weeks after Ki20227 treatment was terminated (Figure 2H). The repopulated macrophages were located in the adventitia and in the close vicinity of medial SMCs, similar to untreated WT mice (Figure 2I). To evaluate how these cells were replenished, we assessed macrophage repopulation in lethally irradiated CD45.2⁺ mice transplanted with congenic CD45.1⁺ bone marrow (BM) cells, both before and after Ki20227 treatment (Figure 2J). In agreement with previous findings (Hashimoto et al., 2013), recipient mice achieved almost complete donor chimerism among blood monocytes 1 month after transplantation. The donor chimerism of aortic monocytes remained >85% both before and after Ki20227 treatment, confirming that they derive from BM cells (Figure 2J). Arterial macrophages were replaced by donor BM cells to the proportion of 64.85% of the population at steady state and 80.48% after depletion, respectively. Notably, these newly replaced BM-derived macrophages were able to reverse arterial remodelling (Figures 2K–2N) and function (Figures 2O and 2P).

Finally, we examined the impact of arterial macrophage depletion on arterial stiffness in atherosclerotic-prone apolipoprotein E-deficient (*Apoe*^{−/−}) mice. Previous studies in such mice had shown that arterial stiffness precedes the formation of atherosclerotic lesions (Gotschy et al., 2013). Consistent with these findings, the descending aortas of 18-week-old *Apoe*^{−/−} mice exhibited increased arterial stiffness as measured by our tensile strength assay and negligible atherosclerosis (Figures S1L–S1N). Treatment of *Apoe*^{−/−} mice with Ki20227 abrogated residual arterial macrophages and further exacerbated arterial stiffness and collagen deposition in the adventitia with no alterations in systemic blood pressure (Figures 2Q–2Y).

These results show that the alterations in vessel structure observed after depletion of arterial macrophages are accompanied by changes in aortic biomechanics and imply that the maintenance of arterial integrity and function depends on the presence of arterial macrophages under both steady-state and pathological conditions.

The Predominant Aortic Macrophage Population in the Steady State Expresses the Lymphatic Hyaluronan Receptor LYVE-1

Because tissue macrophages are phenotypically and functionally heterogeneous (Varol et al., 2015), we considered the possibility that those responsible for regulating arterial homeostasis might represent a distinct phenotypic subpopulation. We focused on their expression of LYVE-1, the main hyaluronan receptor in lymphatic vessel endothelium that mediates docking and entry of leukocytes (Jackson, 2018; Johnson et al., 2017), but which is also expressed in certain subsets of M2-like tissue macrophages (Cho et al., 2007; Ensan et al., 2016; Faraco et al., 2016; Pinto et al., 2012; Xu et al., 2007). Consistent with

the recent report by Ensan et al. (2016), LYVE-1⁺ cells were found to be abundant throughout the entire surface of normal adult mouse aortas (Figure 3A). Flow cytometric analysis revealed that MerTK⁺CD64⁺F4/80⁺CD11b⁺ aortic macrophages were predominantly LYVE-1⁺ as opposed to LYVE-1[−] (Figure 3B). LYVE-1⁺ macrophages were also positive for the M2 macrophage markers CD163 and CD206 (Figure S2A; Pinto et al., 2012). Further analysis of MHCII expression showed that the aortas contained equal proportions of MHCII⁺ and MHCII[−] LYVE-1⁺ macrophages (Figure 3B). LYVE-1⁺ macrophages resided exclusively within the adventitia and were absent from the media and intima (Figure 3C), whereas both MHCII[−] and MHCII⁺ LYVE-1⁺ macrophages were often found spatially associated with the media (Figures 3D and 3E). In contrast, LYVE-1[−] macrophages were rarely observed in the aortic adventitia at steady state (Figure 3D). Further examination of the spatial distribution of macrophages within the arterial layers by flow cytometry confirmed that LYVE-1⁺ macrophage numbers were markedly higher in the adventitia than in the intima and media (Figure 3F).

LYVE-1 expression in these arterial macrophages is apparently not required for their development and persistence in the adult aorta, at least under normal condition since CD68⁺ macrophages remained abundant in the adventitial layer of *Lyve1*^{−/−} mice, in close contact with medial SMCs and expressed CD163 (Figures S2B and S2C). In line with the report by Ensan et al. (2016), we detected CX3CR1⁺ macrophages in aortas of *Cx3cr1*^{gfp/+} mice (Figures S2D and S2E; Ensan et al., 2016). However, only a fraction of LYVE-1⁺ macrophages expressed CX3CR1 (Figures S2D and S2E). Analysis of MaFIA mouse aortic sections confirmed that LYVE-1⁺ macrophages expressed CSF-1R (Figure 3G) and flow cytometric analysis revealed that CSF-1R expression was more abundant on the surface of aortic LYVE-1⁺ macrophages than LYVE-1[−] macrophages (Figure 3H). Consistent with the role of CSF-1R signaling in maintenance of arterial MerTK⁺CD64⁺ macrophage survival (Figures 1G and 1H), treatment for 2 weeks with Ki20227 resulted in a profound depletion of LYVE-1⁺ macrophages in aortas of WT mice (Figures 3I and 3J). These findings raise the possibility that depletion of these cells may contribute to the arterial stiffness and collagen deposition observed after Ki20227 treatment.

LYVE-1⁺ Macrophages Are Universally Associated with Blood Vessels Invested by Smooth Muscle Cells in Both Mouse and Human Tissues

We assessed whether the LYVE-1⁺ macrophage population also lines the blood vasculature of other tissues. To investigate the 3D spatial distribution of LYVE-1⁺ cells in mouse skin, we utilized multi-photon microscopy to visualize ear skin whole-mount preparations. LYVE-1⁺ cells first appeared below the uppermost part of the dermis (~38 μm) and persisted throughout the deeper dermis (below 80 μm; Figure 4A). We also observed that some but not all LYVE-1⁺ cells aligned with each other to form “train track” structures (Figure 4A and Video S1), suggesting that such cells were associated with vessels. A subset of LYVE-1⁺ cells was indeed arranged along large CD31⁺ vessels in the deeper dermis (below ~38 μm) whereas no LYVE-1⁺ cells were associated with smaller CD31⁺ vessels or initial lymphatic in the uppermost dermis (0–34 μm; Figure 4A and Video S1). In

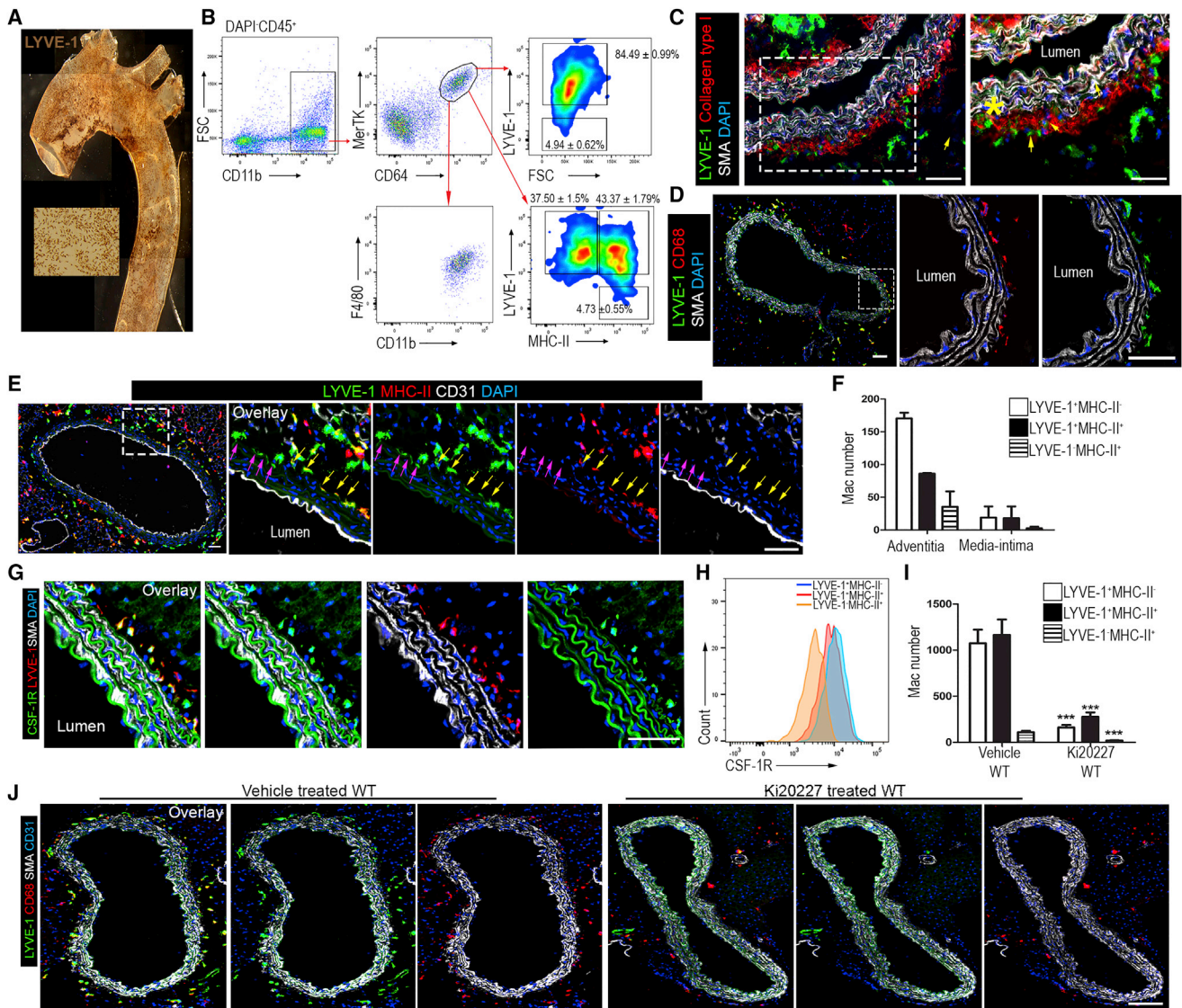


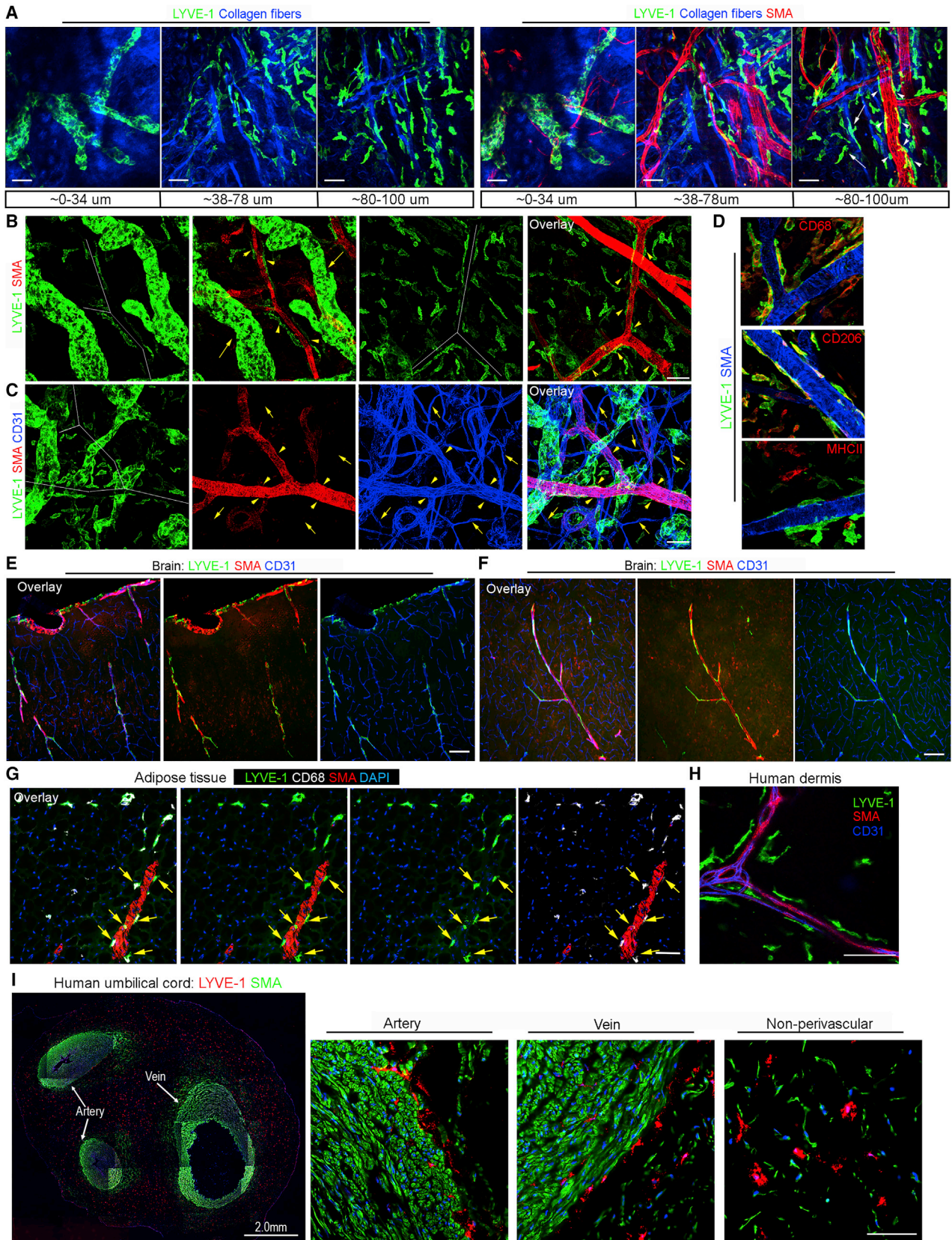
Figure 3. Phenotype of Aortic Macrophages

(A) Aorta whole mount stained for LYVE-1.
 (B) Gating strategy for aortic macrophages (mean \pm SEM, n = 6). Numbers denotes percentage of macrophage subsets.
 (C) Aortic sections stained for Col I, SMA, and LYVE-1 (arrows). Asterisk denotes SMA⁺ media.
 (D) Aortic sections stained for LYVE-1, CD68, and SMA.
 (E) Aortic sections stained for LYVE-1, MHC-II, and CD31. Pink arrows and yellow arrows indicate LYVE-1⁺MHC-II⁻ and LYVE-1⁺MHC-II⁺ macrophages, respectively.
 (F) Number of macrophage subsets (mean \pm SEM, n = 2).
 (G) Aortic sections of MaFIA mice showing CSF-1R expression on LYVE-1⁺ macrophages.
 (H) CSF-1R expression by macrophage subsets.
 (I and J) WT mice received Ki20227 for 2 weeks.
 (I) Aortic macrophages number (mean \pm SEM; n = 13 per group).
 (J) LYVE-1⁺ macrophages in aortic sections.
 Data are collected from 2–3 independent experiments. ***p < 0.0005. Scale bar = 50 μ m except (J) = 100 μ m. See also Figure S2.

the skin, the blood vasculature mainly consists of arterioles and venules that are surrounded by SMCs expressing smooth muscle actin (SMA) and capillaries that are covered by SMA⁻ pericytes. Triple staining for SMA, LYVE-1, and CD31 revealed that LYVE-1⁺ cells lined vessels invested with SMA⁺ SMCs but not the smaller SMA⁻ capillaries (Figures 4B and 4C and

Video S2). Co-staining of whole-mount tissues with CD68, CD206, and CSF-1R also confirmed that LYVE-1⁺ macrophages underlined perivascular SMCs in skin (Figures 4D and S3A).

Consistent with recent observations in the mouse brain (Faraco et al., 2016), LYVE-1⁺ macrophages were associated with pial, penetrating parenchymal and meningeal SMC⁺ vessels



but not SMC⁻ vessels (Figures 4E, 4F, S3C, and S3D). LYVE-1⁺ macrophages also lined SMA⁺ blood vessels in other vascularized mouse tissues including adipose tissues and tracheae (Figures 4G and S3B). LYVE-1⁺ macrophages were also found on human SMA⁺ vasculature in the dermis of abdominal skin (Figures 4H and S3E) and in umbilical cord (Figure 4I). These data reveal the exclusive distribution of LYVE-1⁺ macrophages in the adventitia of SMA⁺ large blood vessels and provide preliminary evidence that this subset of perivascular macrophages is conserved across different tissues and species.

LYVE-1⁺ and LYVE-1⁻ Aortic Macrophages Are Functionally Distinct

To gain insight into the functions of arterial LYVE-1⁺ and LYVE-1⁻ macrophages, we performed gene expression profiling using RNA sequencing. Transcriptional profiling revealed 288 genes that were differentially expressed between aortic LYVE-1⁺ and LYVE-1⁻ macrophages. Among them, LYVE-1⁺ macrophages displayed 125 positively regulated and 163 negatively regulated genes relative to LYVE-1⁻ macrophages (Figure 5A and Table S1). We performed functional enrichment analyses on the two groups of differentially expressed genes to account for the biological processes in which they are involved, based on Gene Ontology annotation. We found that genes upregulated in LYVE-1⁻ macrophages were enriched for terms related to immune responses and antigen processing whereas genes that were more abundant in LYVE-1⁺ macrophages were enriched for terms related to a broad range of homeostatic processes including metabolism, angiogenesis, elastin catabolism, cardiac muscle growth, and communication (Figures 5B and 5C and Table S2). These data reveal that LYVE-1⁺ and LYVE-1⁻ macrophages are functionally distinct with LYVE-1⁺ macrophages, having more of an involvement with tissue homeostasis.

We therefore hypothesized that LYVE-1⁺ macrophages are the homeostatic regulators of arterial function. To address this hypothesis, *Lyve1^{cre/cre}* mice (Pham et al., 2010) were crossed with *Csf1r* floxed mice (*Csf1r^{flox/flox}*) (Li et al., 2006) to generate *Lyve1^{wt/cre};Csf1r^{flox/flox}* mice, in which *Csf1r* was specifically depleted in all LYVE-1-expressing cells. Since LYVE-1⁺ macrophages depend on the CSF-1R pathway, LYVE-1⁺ macrophages are depleted in *Lyve1^{wt/cre};Csf1r^{flox/flox}* mice. Such mice showed depletion of LYVE-1⁺ macrophages in the aortas regardless of their MHC class II expression whereas LYVE-1⁻ macrophages, blood, and aortic monocytes were not affected (Figures 5D–5I). Using this mouse model lacking specifically LYVE-1⁺ macrophages, we determined the consequences of their absence on

arterial stiffness and ECM remodelling. Luminal diameter (Figure 5K), adventitial area (Figures 5J and 5L), and collagen deposition (Figures 5M and 5N) were increased in *Lyve1^{wt/cre};Csf1r^{flox/flox}* mice compared to control *Csf1r^{flox/flox}* mice. These structural modifications were accompanied by an increase in aortic wall stiffness without any changes in maximal contractile force (Figures 5O and 5P). Similar to WT mice treated with Ki20227, blood pressure was not altered in *Lyve1^{wt/cre};Csf1r^{flox/flox}* mice (Figures 5Q–5S). Next, we investigated whether the absence of LYVE-1⁺ macrophages leads to similar collagen deposition in tissues other than aorta, specifically intestine and esophagus. Intestinal macrophages were predominantly LYVE-1⁻ although occasional LYVE-1⁺ macrophages were seen in the submucosal layer (data not shown). In contrast, LYVE-1⁺ macrophages were abundant in murine esophagus and were located mostly in the muscularis mucosa where SMCs reside and in the connective tissue of the submucosa (Figure S4A). Similar to aortic macrophages, esophageal macrophages were depleted in *Lyve1^{wt/cre};Csf1r^{flox/flox}* mice (Figure S4A). Moreover, the absence of esophageal LYVE-1⁺ macrophages in these mice resulted in accumulation of collagen in the muscularis mucosa and submucosa (Figures S4B–S4D).

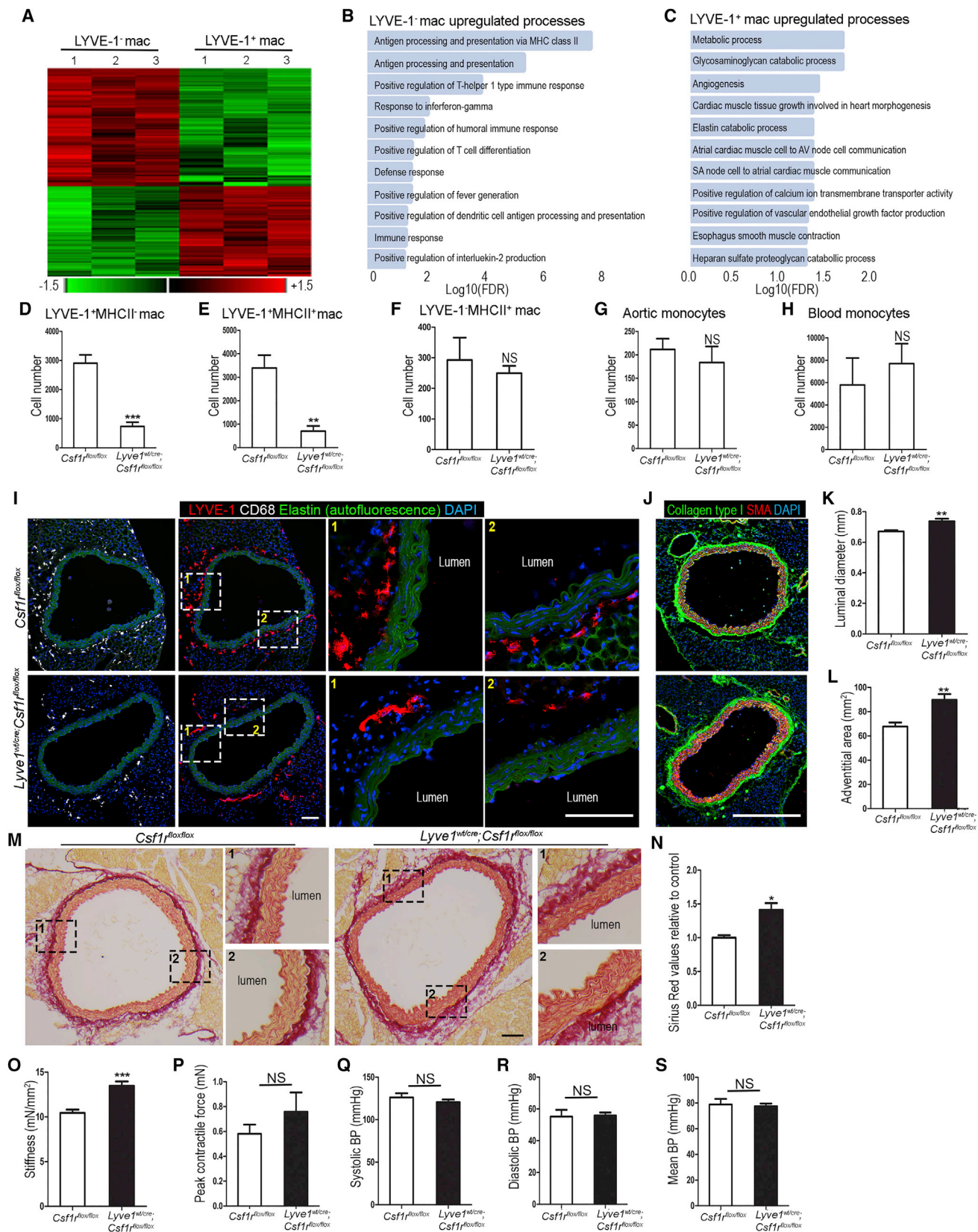
These results highlight the unique function of LYVE-1⁺ macrophages in preventing arterial stiffness and collagen deposition. They also indicate that LYVE-1⁺ macrophage association with SMCs is not restricted to vascular SMCs and that the control of collagen deposition by LYVE-1⁺ macrophages is likely a general phenomenon and not one specific to the aorta.

Engagement of LYVE-1⁺ Macrophages with HA on SMCs and MMP-9-Dependent Proteolysis Are Required for the Regulation of Arterial Collagen Production

Ex and *in vivo* analysis of the phagocytic capacity of aortic LYVE-1⁺ and LYVE-1⁻ macrophages revealed that both macrophage subsets displayed similar phagocytic properties (Figures S5A and S5B). These data indicate that LYVE-1⁺ macrophages contributed to arterial homeostatic function via a tissue process other than phagocytosis. Since vascular integrity and contractile function are regulated by ECM proteins produced largely by SMCs (Wagenseil and Mecham, 2009), we reasoned that LYVE-1⁺ macrophages might exert their effects by modulating SMC function. We first examined the effect of LYVE-1⁺ macrophages on the production of collagen by primary cultured murine aortic SMCs *in vitro* (Figure S5C). Because of the limited recoveries of LYVE-1⁺ and LYVE-1⁻ macrophages from aortas after cell sorting, we instead used macrophages sorted from mouse adipose tissues for these *in vitro* co-culture systems. LYVE-1⁺

Figure 4. LYVE-1⁺ Macrophages Are Associated with Vascular SMCs

(A) Extended views of ear whole mounts for LYVE-1, CD31, and collagen (second harmonic generation), starting from the dermoepidermal junction. White arrows and arrowheads indicate non-perivascular and perivascular LYVE-1⁺ macrophages, respectively.
 (B and C) Confocal images of ear whole mount stained for LYVE-1, SMA (B), and CD31 (C). Dotted white lines illustrate the train track patterning by LYVE-1⁺ cells. Yellow arrowheads indicate perivascular LYVE-1⁺ macrophages while yellow arrows denote initial lymphatics in (B) and capillaries in (C).
 (D) LYVE-1⁺ cells lining SMA⁺ blood vessels in ear whole mount were CD68⁺CD206⁺MHC-II⁻.
 (E and F) LYVE-1⁺ macrophages are associated with pial, pial penetrating (E), and parenchymal (F) SMC⁺ vessels of the brain.
 (G) Adipose tissue sections stained for LYVE-1, CD68, SMA, and DAPI. Yellow arrows indicate perivascular macrophages.
 (H) Human skin stained for LYVE-1, SMA, and CD31.
 (I) Human umbilical cord sections stained for LYVE-1 and SMA identified LYVE-1⁺ cells surrounding SMA⁺ arteries and vein.
 Images are representative of at least 3–10 mice/human samples for each condition examined. Scale bar = 50 μm except (E), (F), (H), and (I) = 100 μm. See also Figure S3.



(legend on next page)

macrophages were the predominant resident macrophage population in adipose tissue, exhibited higher expression of CSF-1R compared to LYVE-1⁻ macrophages, and expressed genes enriched for terms related to key homeostatic processes, similar to their aortic LYVE-1⁺ macrophage counterparts (Figures S5D–5H and Tables S3 and S4). While addition of LYVE-1⁻ macrophages to cultured SMCs exerted no effect on the amounts of Col I (the most abundant ECM protein in aortic wall), addition of such LYVE-1⁺ macrophages induced a significant reduction (Figures 6A and 6B). These data show that LYVE-1⁺ macrophages have a unique ability to modulate the collagen content in vascular SMCs.

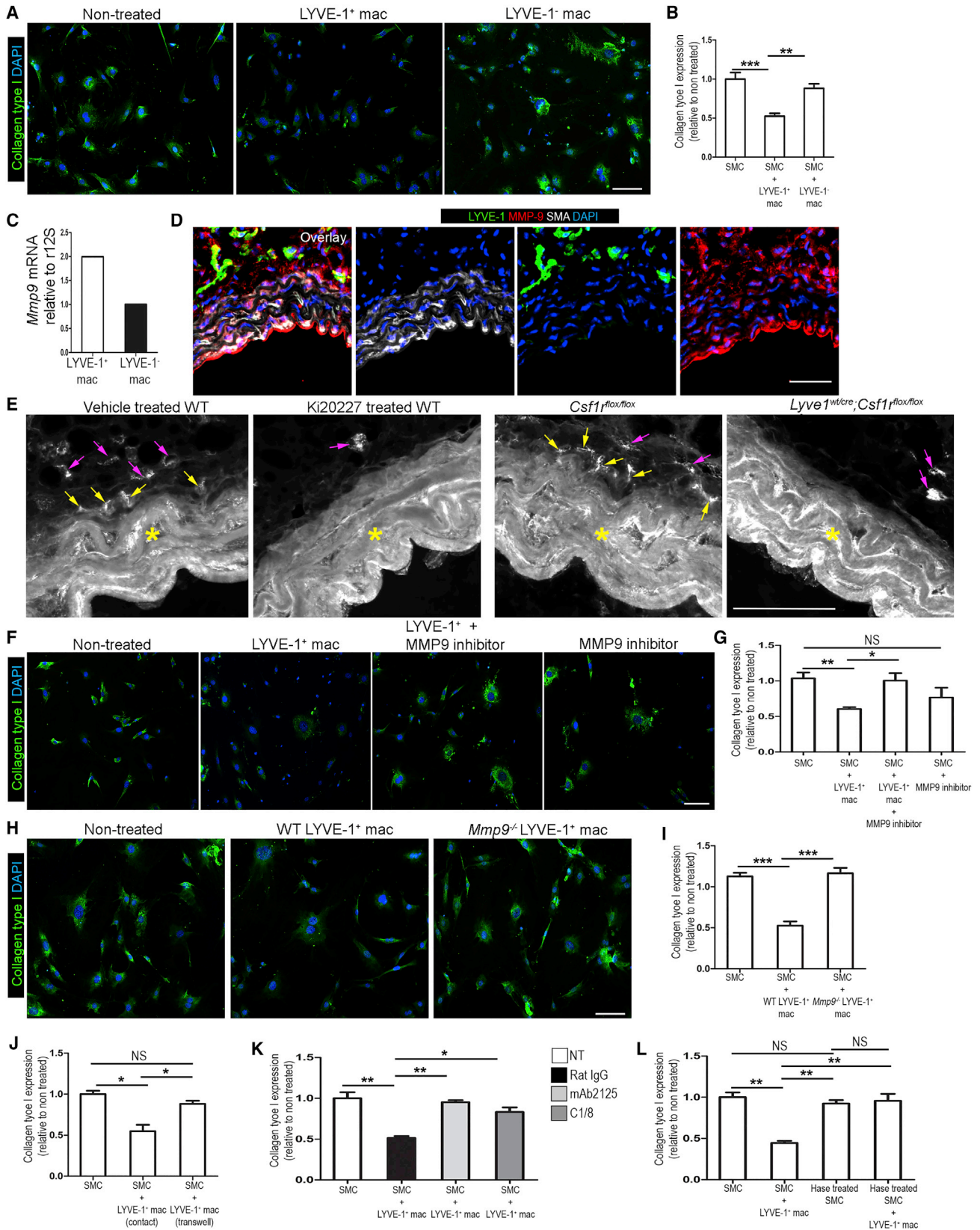
We next investigated the mechanisms by which LYVE-1⁺ macrophages regulate SMC collagen *in vitro*. The reduced production of Col I in SMCs observed in the presence of LYVE-1⁺ macrophages likely resulted from protein degradation rather than transcriptional regulation, since we did not observe marked differences in *Col1a1* gene expression (Figure S5i). MMPs contribute to vascular ECM homeostasis through the degradation of ECM proteins and also prevent overload of ECM components (Castro et al., 2011). The depletion of MMP-9 in rodents is known to aggravate arterial stiffness and increases vascular collagen content (Flamant et al., 2007). Macrophages have been shown to express MMP-9 (Yabluchanskiy et al., 2013). In our study, aortic adventitial *Mmp9* mRNA expression was significantly decreased following macrophage depletion (Figure 2B) and higher expression of *Mmp9* was detected in LYVE-1⁺ macrophages compared to LYVE-1⁻ macrophages sorted from adult WT adipose tissues (Figure 6C). Immunofluorescence analysis of WT aortic sections revealed MMP-9 expression in adventitial LYVE-1⁺ macrophages and in the intima, with minimal amounts being detected in the medial SMCs (Figure 6D). Next, we assayed for MMP-9 activity in aortic sections by gelatin-based *in situ* zymography. We detected proteolytic activity in the periaortic fat, as well as the adventitial and medial layers in WT and control *Csf1r^{fllox/fllox}* mice. In contrast, this activity was markedly reduced in the periaortic fat and adventitial layers of Ki20227-treated WT mice and *Lyve1^{wt/cre};Csf1r^{fllox/fllox}* mice (Figure 6E) whereas it remained unaltered in the media of these mice. These findings suggested that LYVE-1⁺ macrophages might utilize MMP-9 to degrade SMC collagen and thus we initially evaluated the effects of adding a selective MMP-9 inhibitor in our LYVE-1⁺ macrophage and SMC *in vitro* co-culture system. Addition of the MMP-9 inhibitor to cultured SMCs alone had no effect on Col I expression (Figures 6F and 6G). In contrast,

when added to SMCs co-cultured with LYVE-1⁺ macrophages, the reduction in Col I amounts exerted by the latter was partly reversed (Figures 6F and 6G), indicating that MMP-9 derived from these LYVE-1⁺ macrophages was responsible for the Col I degradation. This was confirmed when LYVE-1⁺ macrophages sorted from MMP-9-deficient mice were cultured with SMCs, since these had no such effect on Col I (Figures 6H and 6I). Therefore, we conclude that LYVE-1⁺ macrophages regulate collagen content in vascular SMCs, to a significant degree via MMP-9-dependent proteolysis. However, the collagen degradative activity of LYVE-1⁺ macrophages was not recapitulated when purified pro- or active forms of MMP-9 were added instead to SMCs (Figure S6A), suggesting that such macrophages played an additional potentiating role in the process.

With regard to this possibility, recent reports have shown that MMP-9 can act pericellularly through its interaction with cell surface components (Murphy and Nagase, 2011). We hypothesized that MMP-9 may be sequestered on the surface of LYVE-1⁺ macrophages and that a direct macrophage:SMC cell:cell interaction may be required to focus its proteolytic activity on Col I. When LYVE-1⁺ macrophages were prevented from making physical contact with vascular SMCs in a transwell system, they lost the capacity to degrade SMC collagen (Figure 6J). We then sought to identify the components required for this interaction between LYVE-1⁺ macrophages and SMCs. Since MMP-9 can localize pericellularly through its binding to β -integrin and CD44 (Redondo-Muñoz et al., 2008; Yu and Stamenkovic, 2000), we evaluated the involvement of these receptors using specific blocking mAbs. Neither blocking integrin beta-1 (ITGB1) nor CD44 affected the capacity of LYVE-1⁺ macrophages to alter collagen expression in SMCs (Figure S6B). Since CD44 expression was comparable in LYVE-1⁺ and LYVE-1⁻ macrophages (Figure S6C) and LYVE-1 (in common with CD44) is a receptor for HA, we went on to block LYVE-1 with two mAbs, 2125 and C1/8, that specifically target the LYVE-1 HA binding site (Johnson et al., 2017). Degradation of collagen in SMCs by LYVE-1⁺ macrophages was abrogated in the presence of either of these mAbs (Figure 6K). These results suggested either that LYVE-1 sequesters MMP-9 via its HA-binding site or that the receptor mediates the interaction between macrophages and SMCs required for MMP-9-dependent collagen degradation, by engaging with HA in the SMC pericellular matrix (Figure 6K). To distinguish between these two possibilities, we specifically depleted the pericellular HA on SMCs by hyaluronidase treatment (Figure S6D). Such depletion completely

Figure 5. Specific Depletion of Aortic-Resident LYVE-1⁺ Macrophages Leads to Arterial Wall Remodelling and Dysfunction

- (A–C) Transcriptome profiling of aortic LYVE-1⁺ and LYVE-1⁻ macrophages.
 (A) Heatmap showing differential expressed genes between aortic LYVE-1⁺ and LYVE-1⁻ macrophages.
 (B and C) Histogram of aortic LYVE-1⁺ and LYVE-1⁻ macrophages with specific gene functions based on GO classification.
 (D–S) Aortas from 16-week-old *Lyve1^{wt/cre};Csf1r^{fllox/fllox}* and *Csf1r^{fllox/fllox}* mice were obtained for analysis.
 (D–H) Macrophages and monocytes number determined by flow cytometry (mean \pm SEM; n = 6–8 per group).
 (I) Aortic sections immunostained for LYVE-1 and CD68. Media elastic lamella is auto-fluorescent (green). Inserts show high magnification.
 (J) Immunostaining for Col I and SMA.
 (K and L) Luminal diameter (K) and adventitial area (L) (mean \pm SEM; n = 5 per group).
 (M) Sirius red-stained aortic sections.
 (N) Quantification of aorta collagen content by Sirius red (mean \pm SEM, n = 7).
 (O and P) Stiffness (O) and maximal contractile force (P) in response to KCl stimulus (mean \pm SEM with n = 6–11 mice).
 (Q–S) Systolic (Q), diastolic (R), and mean (S) blood pressure (mean \pm SEM, n = 5–7 per group).
 Data are collected from 2–3 independent experiments. *p < 0.05; **p < 0.005; ***p < 0.0005. Scale bar = 100 μ m. See also Figure S4.



(legend on next page)

abrogated the collagenolytic effect of LYVE-1⁺ macrophages (Figure 6L), confirming that these cells exert their critical regulation of matrix homeostasis and vessel mechanics through HA-dependent SMC adhesion.

DISCUSSION

Despite initial studies reporting the occurrence of resident arterial macrophages under steady-state conditions (Ensan et al., 2016; Faraco et al., 2016; Galkina et al., 2006; Jongstra-Bilen et al., 2006) and their functional involvement during inflammation and vascular diseases (Fung and Helisch, 2012; Simons and Eichmann, 2015; Swirski et al., 2016), ours unveils that these cells sustain large blood vessel functional homeostasis, in part by modulating the ECM environment.

The abnormal remodelling of aortic ECM has major detrimental consequences including contractile dysfunction, aberrant mechanosensing, and compromised arterial integrity (collectively referred to as arterial stiffness) that eventually diminish the capacity of vessels to accommodate cardiac load (Kohn et al., 2015). Several studies have reported the prognostic value of arterial stiffness in patient- and general population-based cohorts as an independent predictor of cardiovascular events, morbidity, and all-cause mortality (Palombo and Koza-kova, 2016). In line with these epidemiological findings, animal models of arterial stiffness associated with ECM remodelling have revealed fatal cardiovascular diseases and complications such as ischemia, aneurysms, and atherosclerosis (Kothapalli et al., 2012; Lacolley et al., 2014). We show here that depletion of arterial macrophages in healthy aorta led to reduced contractile function and increased aortic stiffness and collagen production. These defects were reversed by functional replenishment of arterial macrophages that derived from BM cells. Moreover, arterial stiffness associated with atherosclerosis was exacerbated when arterial macrophages were depleted. In both models, arterial stiffness was not associated with any changes in blood pressure. This is consistent with data showing that blood pressure is not modified despite marked arterial remodelling and/or arterial stiffness as observed in the well-established angiotensin II-induced aneurysm *Apoe*^{-/-} mouse model (Daugherty et al., 2000) and in aged WT mice (Francia et al., 2004). Our data reveal arterial macrophages as regulators of vascular homeostatic function that have potentially beneficial

effects on arterial stiffness and cardiovascular diseases through their ability to regulate ECM production. He et al. (2016) have demonstrated the importance of perivascular macrophages residing in SMC⁻ small blood vessels, namely capillaries, for the control of vascular permeability. Therefore, our study along with this latter report support the notion that under physiological conditions, the blood vasculature is actively maintained and highlights the functional diversity and specialization of perivascular macrophages, depending on the type of vessels in which they reside.

Functional diversity also seems to be apparent within the same type of vessel, likely reflecting a high degree of macrophage heterogeneity. In our study, assessment of LYVE-1 expression in the steady state revealed that the aorta contains two distinct populations of macrophages, namely LYVE-1⁻ and LYVE-1⁺ macrophages, of which the latter are the most numerous residents. Additional heterogeneity among aortic macrophages was further unveiled by including the functional marker MHCII. The differential expression of MHCII on the surface of LYVE-1⁺ macrophages further sub-divided this population into LYVE-1⁺MHCII⁺ and LYVE-1⁺MHCII⁻, whereas all LYVE-1⁻ macrophages were MHCII⁺. Furthermore, we showed that some but not all LYVE-1⁺ macrophages express CX3CR1. Similar subpopulations of tissue-resident macrophages based on MHCII and CX3CR1 marker expression have been described for dermal, cardiac, and intestinal lamina propria-resident macrophages (Epelman et al., 2014; Tamoutounour et al., 2012, 2013). Hence, there is more phenotypic heterogeneity among arterial macrophages than previously appreciated (Ensan et al., 2016).

Aortic LYVE-1⁻ and LYVE-1⁺ macrophage subpopulations appear to have distinct functions within the vessel wall. Supporting evidence includes our *in vivo* data showing that specific depletion of LYVE-1⁺ macrophages in *Lyve1*^{wt/cre};*Csf1*^{fl/fl/fl/fl} mice resulted in increased arterial stiffness and collagen deposition, our *in vitro* findings showing that LYVE-1⁺ but not LYVE-1⁻ macrophages can act on SMCs to limit collagen expression and our transcriptome profiling of these two subsets of macrophages identifying genes enriched in various local homeostatic processes and immune response in LYVE-1⁺ and LYVE-1⁻ macrophages, respectively. Therefore, our results reveal LYVE-1⁺ macrophages as the key macrophage subset that maintains arterial wall homeostasis by modulating collagen amounts in

Figure 6. LYVE-1⁺ Macrophage Regulation of Collagen Expression by SMCs Relies on MMP-9 and Engagement of HA-LYVE-1 Interaction

(A and B) Primary mouse aortic SMCs co-cultured with LYVE-1⁺ macrophages or LYVE-1⁻ macrophages for 24 hr and stained for collagen type I (mean ± SEM, n = 5–9 per group).

(C) RT-PCR analysis of *Mmp9* on sorted LYVE-1⁺ and LYVE-1⁻ macrophages.

(D) Immunofluorescence for MMP-9, LYVE-1, SMA, and DAPI in WT aortic sections.

(E) Representative images of gelatin *in situ* zymography in aorta sections. Asterisks denote the medial layer. Pink arrows and yellow arrows indicate fluorescence signal from periaortic layer and adventitial layer, respectively.

(F and G) MMP-9 inhibitor was added to SMCs 2 hr prior to add LYVE-1⁺ macrophages for 24 hr (mean ± SEM, n = 2–5 per group).

(H–I) SMCs co-cultured with *Mmp9*^{-/-} and *Mmp9*^{+/+} LYVE-1⁺ macrophages for 24 hr (mean ± SEM, n = 3–4 per group).

(J) SMCs co-cultured with LYVE-1⁺ macrophages via direct contact or separated by transwell membrane (n = 2 per group).

(K) LYVE-1⁺ macrophages were pre-incubated with rat IgG, or anti-LYVE-1 mAb mAb2125, or C1/8 for 30 min prior to add to SMCs for 24 hr (mean ± SEM, n = 2–3 per group).

(L) SMCs were pre-treated with or without hyaluronidase (Hase) for 2 hr and co-cultured with LYVE-1⁺ macrophages in the presence of vehicle or 4-MU for 24 hr (mean ± SEM, n = 3–6 per group). Col I expression was measured by outlining the SMCs with smooth muscle actin staining and normalized to non-treated group. Data are pooled from two independent experiments. *p < 0.05; **p < 0.005; ***p < 0.0005. Scale bar = 100 μm except (D) and (E) = 50 μm. See also Figures S5 and S6 and Tables S3 and S4.

SMCs. It is plausible that LYVE-1⁺ macrophages participate similarly in regulating the blood vasculature of other tissues than the aorta since we found them in skin, trachea, adipose tissue, intestine, and brain. They may also regulate collagen deposition by non-vascular SMCs as suggested by our observation in esophagus.

Our preliminary studies on the mechanisms by which LYVE-1⁺ macrophages regulate collagen expression in SMCs identified MMP-9 as a potential mediator. Although overexpression of MMP-9 has been considered detrimental to various cardiovascular complications (Yabluchanskiy et al., 2013), its beneficial function has been highlighted in early hypertensive arterial stiffness and vein grafting since MMP-9-null mice developed increased vascular stiffness and enhanced collagen deposition (Flamant et al., 2007; Thomas and Newby, 2010), in line with our current study. The negative effect of LYVE-1⁺ macrophages on SMC collagen is unlikely due to increased SMC differentiation because addition of LYVE-1⁺ macrophages to SMCs did not affect the expression of contractile genes in SMCs or their proliferation (data not shown) (Owens et al., 2004). Our data also demonstrate that modulation of collagen expression by LYVE-1⁺ macrophages is dependent on engagement of the receptor with HA on SMCs. Recent work has demonstrated that dendritic cell (DC) trafficking in lymph involves the engagement of LYVE-1 in lymphatic endothelium with HA present in the DC surface glycocalyx (Johnson et al., 2017). Unlike other members of the Link HA receptor superfamily that includes CD44 and Stabilin-2, LYVE-1 is unique in functioning as a disulphide-linked homodimer (Banerji et al., 2016) whose unusual properties allow the receptor to distinguish higher-order HA configurations on cell surfaces from ambient HA in the interstitial matrix through differences in binding avidity (Jackson, 2018). Such properties may well explain how LYVE-1 engages selectively with the SMC HA pericellular matrix to modulate SMC collagen (Jackson, 2018).

In sum, our work addresses previously unanswered questions regarding the homeostatic contribution of arterial macrophages to blood vessels in the adult and their potential ability to regulate vascular tone in the steady state. These biological insights should aid in the development or improvement of existing therapies for the treatment of arterial diseases.

STAR★METHODS

Detailed methods are provided in the online version of this paper and include the following:

- KEY RESOURCES TABLE
- CONTACT FOR REAGENT AND RESOURCE SHARING
- METHOD DETAILS
 - Mice
 - Human materials
 - Animal treatment
 - Transplantation of congenic bone marrow cells
 - Blood pressure measurements
 - Tissue processing, flow cytometry and cell sorting
 - Immunohistochemistry
 - *In vivo* and *in vitro* phagocytosis assay
 - Vascular smooth muscle cells culture and assays
 - *In situ* gelatin zymography for *in vivo* studies

- Data analysis and quantification
- Circumference tensile and contractility tests
- RNA-seq, differential gene expression, and functional enrichment analyses
- Quantitative real-time PCR
- QUANTIFICATION AND STATISTICAL ANALYSIS
- DATA AND SOFTWARE AVAILABILITY

SUPPLEMENTAL INFORMATION

Supplemental Information includes six figures, four tables, and two videos and can be found with this article online at <https://doi.org/10.1016/j.immuni.2018.06.008>.

ACKNOWLEDGMENTS

We thank K. Shortman for critical discussion, Y.H. Lee, Y.S. Yip, and Y.L. Chua for technical assistance, and G.H. Teo and P.E. Hutchinson from Flow Cytometry Lab and E. Koh from Advanced Imaging core facility (Life Science Institute, Immunology programme, NUS) for sharing their expertise. This work was supported by NMRC (CBRGnov094) and NRF grants to V.A., UK Medical research Council funding to D.G.J., and EMBO YIP, SlgN core funding, and Singapore NRF Senior Investigatorship (NRF12017-02) to F.G.

AUTHOR CONTRIBUTIONS

Conception: H.Y.L., S.Y.L., V.A.; research design: H.Y.L., S.Y.L., V.A.; data analysis: H.Y.L., S.Y.L., C.K.T., C.H.T., C.C.G., D.C., S.H.S.C., P.S., S.C., X.N.W., L.H.L., L.A.J., J.L., C.Y.F., A. Bongso, A. Biswas, C.G., M.E., K.P.Y., R.B., J.K.W., Y.T., R.J., S.T., C.C., W.W., M.P., R.E.S., M.C., N.S.T., L.G.N., D.G.J., F.G., V.A.; resource assistance: R.B., M.E., D.G.J., F.G., L.G.N., R.E.S.; writing – draft and editing: H.Y.L., S.Y.L., V.A.; and project administration: V.A.

DECLARATION OF INTERESTS

The authors declare no competing interests.

Received: February 26, 2017

Revised: April 1, 2018

Accepted: June 15, 2018

Published: July 24, 2018

REFERENCES

- Banerji, S., Lawrance, W., Metcalfe, C., Briggs, D.C., Yamauchi, A., Dushek, O., van der Merwe, P.A., Day, A.J., and Jackson, D.G. (2016). Homodimerization of the lymph vessel endothelial receptor LYVE-1 through a redox-labile disulfide is critical for hyaluronan binding in lymphatic endothelium. *J. Biol. Chem.* 291, 25004–25018.
- Burnett, S.H., Kershen, E.J., Zhang, J., Zeng, L., Straley, S.C., Kaplan, A.M., and Cohen, D.A. (2004). Conditional macrophage ablation in transgenic mice expressing a Fas-based suicide gene. *J. Leukoc. Biol.* 75, 612–623.
- Castro, M.M., Tanus-Santos, J.E., and Gerlach, R.F. (2011). Matrix metalloproteinases: targets for doxycycline to prevent the vascular alterations of hypertension. *Pharmacol. Res.* 64, 567–572.
- Cho, C.H., Koh, Y.J., Han, J., Sung, H.K., Jong Lee, H., Morisada, T., Schwendener, R.A., Brekken, R.A., Kang, G., Oike, Y., et al. (2007). Angiogenic role of LYVE-1-positive macrophages in adipose tissue. *Circ. Res.* 100, e47–e57.
- Daugherty, A., Manning, M.W., and Cassis, L.A. (2000). Angiotensin II promotes atherosclerotic lesions and aneurysms in apolipoprotein E-deficient mice. *J. Clin. Invest.* 105, 1605–1612.
- Edgar, R., Domrachev, M., and Lash, A.E. (2002). Gene Expression Omnibus: NCBI gene expression and hybridization array data repository. *Nucleic Acids Res.* 30, 207–210.

- Ensan, S., Li, A., Besla, R., Degousee, N., Cosme, J., Roufaiel, M., Shikatani, E.A., El-Maklizi, M., Williams, J.W., Robins, L., et al. (2016). Self-renewing resident arterial macrophages arise from embryonic CX3CR1(+) precursors and circulating monocytes immediately after birth. *Nat. Immunol.* **17**, 159–168.
- Epelman, S., Lavine, K.J., Beaudin, A.E., Sojka, D.K., Carrero, J.A., Calderon, B., Brija, T., Gautier, E.L., Ivanov, S., Satpathy, A.T., et al. (2014). Embryonic and adult-derived resident cardiac macrophages are maintained through distinct mechanisms at steady state and during inflammation. *Immunity* **40**, 91–104.
- Faraco, G., Sugiyama, Y., Lane, D., Garcia-Bonilla, L., Chang, H., Santisteban, M.M., Racchumi, G., Murphy, M., Van Rooijen, N., Anrather, J., and Iadecola, C. (2016). Perivascular macrophages mediate the neurovascular and cognitive dysfunction associated with hypertension. *J. Clin. Invest.* **126**, 4674–4689.
- Flamant, M., Placier, S., Dubroca, C., Esposito, B., Lopes, I., Chatziantoniou, C., Tedgui, A., Dussault, J.C., and Lehoux, S. (2007). Role of matrix metalloproteinases in early hypertensive vascular remodeling. *Hypertension* **50**, 212–218.
- Francia, P., delli Gatti, C., Bachschmid, M., Martin-Padura, I., Savoia, C., Migliaccio, E., Pellicci, P.G., Schiavoni, M., Lüscher, T.F., Volpe, M., and Cosentino, F. (2004). Deletion of p66shc gene protects against age-related endothelial dysfunction. *Circulation* **110**, 2889–2895.
- Fung, E., and Helisch, A. (2012). Macrophages in collateral arteriogenesis. *Front. Physiol.* **3**, 353.
- Gale, N.W., Prevo, R., Espinosa, J., Ferguson, D.J., Dominguez, M.G., Yancopoulos, G.D., Thurston, G., and Jackson, D.G. (2007). Normal lymphatic development and function in mice deficient for the lymphatic hyaluronan receptor LYVE-1. *Mol. Cell. Biol.* **27**, 595–604.
- Galkina, E., Kadl, A., Sanders, J., Varughese, D., Sarembock, I.J., and Ley, K. (2006). Lymphocyte recruitment into the aortic wall before and during development of atherosclerosis is partially L-selectin dependent. *J. Exp. Med.* **203**, 1273–1282.
- Gautier, E.L., Shay, T., Miller, J., Greter, M., Jakubzick, C., Ivanov, S., Helft, J., Chow, A., Elpek, K.G., Gordonov, S., et al.; Immunological Genome Consortium (2012). Gene-expression profiles and transcriptional regulatory pathways that underlie the identity and diversity of mouse tissue macrophages. *Nat. Immunol.* **13**, 1118–1128.
- Ginhoux, F., and Jung, S. (2014). Monocytes and macrophages: developmental pathways and tissue homeostasis. *Nat. Rev. Immunol.* **14**, 392–404.
- Gotschy, A., Bauer, E., Schrod, C., Lykowsky, G., Ye, Y.X., Rommel, E., Jakob, P.M., Bauer, W.R., and Herold, V. (2013). Local arterial stiffening assessed by MRI precedes atherosclerotic plaque formation. *Circ Cardiovasc Imaging* **6**, 916–923.
- Hashimoto, D., Chow, A., Noizat, C., Teo, P., Beasley, M.B., Leboeuf, M., Becker, C.D., See, P., Price, J., Lucas, D., et al. (2013). Tissue-resident macrophages self-maintain locally throughout adult life with minimal contribution from circulating monocytes. *Immunity* **38**, 792–804.
- He, H., Mack, J.J., Güç, E., Warren, C.M., Squadrito, M.L., Kilarski, W.W., Baer, C., Freshman, R.D., McDonald, A.I., Ziyad, S., et al. (2016). Perivascular macrophages limit permeability. *Arterioscler. Thromb. Vasc. Biol.* **36**, 2203–2212.
- Hume, D.A., and MacDonald, K.P. (2012). Therapeutic applications of macrophage colony-stimulating factor-1 (CSF-1) and antagonists of CSF-1 receptor (CSF-1R) signaling. *Blood* **119**, 1810–1820.
- Jackson, D.G. (2018). Hyaluronan in the lymphatics: The key role of the hyaluronan receptor LYVE-1 in leucocyte trafficking. *Matrix Biol.* Published online February 6, 2018. S0945-053X(17)30484-5.
- Johnson, L.A., Banerji, S., Lawrence, W., Gileadi, U., Prota, G., Holder, K.A., Roshorn, Y.M., Hanke, T., Cerundolo, V., Gale, N.W., and Jackson, D.G. (2017). Dendritic cells enter lymph vessels by hyaluronan-mediated docking to the endothelial receptor LYVE-1. *Nat. Immunol.* **18**, 762–770.
- Jongstra-Bilen, J., Haidari, M., Zhu, S.N., Chen, M., Guha, D., and Cybulsky, M.I. (2006). Low-grade chronic inflammation in regions of the normal mouse arterial intima predisposed to atherosclerosis. *J. Exp. Med.* **203**, 2073–2083.
- Kohn, J.C., Lampi, M.C., and Reinhart-King, C.A. (2015). Age-related vascular stiffening: causes and consequences. *Front. Genet.* **6**, 112.
- Kothapalli, D., Liu, S.L., Bae, Y.H., Monslow, J., Xu, T., Hawthorne, E.A., Byfield, F.J., Castagnino, P., Rao, S., Rader, D.J., et al. (2012). Cardiovascular protection by ApoE and ApoE-HDL linked to suppression of ECM gene expression and arterial stiffening. *Cell Rep.* **2**, 1259–1271.
- Kubota, Y., Takubo, K., Shimizu, T., Ohno, H., Kishi, K., Shibuya, M., Saya, H., and Suda, T. (2009). M-CSF inhibition selectively targets pathological angiogenesis and lymphangiogenesis. *J. Exp. Med.* **206**, 1089–1102.
- Lacolley, P., Thornton, S.N., and Bezie, Y. (2014). Animal models for studies of arterial stiffness. In *Blood Pressure and Arterial Wall Mechanics in Cardiovascular Diseases*, M.E. Safar, M.F. O'Rourke, and E.D. Frohlich, eds. (London: Springer London), pp. 63–74.
- Li, J., Chen, K., Zhu, L., and Pollard, J.W. (2006). Conditional deletion of the colony stimulating factor-1 receptor (c-fms proto-oncogene) in mice. *Genesis* **44**, 328–335.
- Murphy, G., and Nagase, H. (2011). Localizing matrix metalloproteinase activities in the pericellular environment. *FEBS J.* **278**, 2–15.
- Owens, G.K., Kumar, M.S., and Wamhoff, B.R. (2004). Molecular regulation of vascular smooth muscle cell differentiation in development and disease. *Physiol. Rev.* **84**, 767–801.
- Palombo, C., and Kozakova, M. (2016). Arterial stiffness, atherosclerosis and cardiovascular risk: Pathophysiologic mechanisms and emerging clinical indications. *Vascul. Pharmacol.* **77**, 1–7.
- Pham, T.H., Baluk, P., Xu, Y., Grigorova, I., Bankovich, A.J., Pappu, R., Coughlin, S.R., McDonald, D.M., Schwab, S.R., and Cyster, J.G. (2010). Lymphatic endothelial cell sphingosine kinase activity is required for lymphocyte egress and lymphatic patterning. *J. Exp. Med.* **207**, 17–27.
- Pinto, A.R., Paolicelli, R., Salimova, E., Gospocic, J., Slonimsky, E., Bilbao-Cortes, D., Godwin, J.W., and Rosenthal, N.A. (2012). An abundant tissue macrophage population in the adult murine heart with a distinct alternatively-activated macrophage profile. *PLoS ONE* **7**, e36814.
- Redondo-Muñoz, J., Ugarte-Berzal, E., García-Marco, J.A., del Cerro, M.H., Van den Steen, P.E., Opendakker, G., Terol, M.J., and García-Pardo, A. (2008). Alpha4beta1 integrin and 190-kDa CD44v constitute a cell surface docking complex for gelatinase B/MMP-9 in chronic leukemic but not in normal B cells. *Blood* **112**, 169–178.
- Simons, M., and Eichmann, A. (2015). Molecular controls of arterial morphogenesis. *Circ. Res.* **116**, 1712–1724.
- Swirski, F.K., Robbins, C.S., and Nahrendorf, M. (2016). Development and Function of Arterial and Cardiac Macrophages. *Trends Immunol.* **37**, 32–40.
- Tamoutounour, S., Henri, S., Lelouard, H., de Bovis, B., de Haar, C., van der Woude, C.J., Woltman, A.M., Reyat, Y., Bonnet, D., Sichien, D., et al. (2012). CD64 distinguishes macrophages from dendritic cells in the gut and reveals the Th1-inducing role of mesenteric lymph node macrophages during colitis. *Eur. J. Immunol.* **42**, 3150–3166.
- Tamoutounour, S., Guillems, M., Montanana Sanchis, F., Liu, H., Terhorst, D., Malosse, C., Pollet, E., Ardouin, L., Luche, H., Sanchez, C., et al. (2013). Origins and functional specialization of macrophages and of conventional and monocyte-derived dendritic cells in mouse skin. *Immunity* **39**, 925–938.
- Tan, C.K., Tan, E.H., Luo, B., Huang, C.L., Loo, J.S., Choong, C., and Tan, N.S. (2013). SMAD3 deficiency promotes inflammatory aortic aneurysms in angiotensin II-infused mice via activation of iNOS. *J. Am. Heart Assoc.* **2**, e000269.
- Thomas, A.C., and Newby, A.C. (2010). Effect of matrix metalloproteinase-9 knockout on vein graft remodelling in mice. *J. Vasc. Res.* **47**, 299–308.
- Tsamis, A., Krawiec, J.T., and Vorp, D.A. (2013). Elastin and collagen fibre microstructure of the human aorta in ageing and disease: a review. *J. R. Soc. Interface* **10**, 20121004.

- Vafaie, F., Yin, H., O'Neil, C., Nong, Z., Watson, A., Arpino, J.M., Chu, M.W., Wayne Holdsworth, D., Gros, R., and Pickering, J.G. (2014). Collagenase-resistant collagen promotes mouse aging and vascular cell senescence. *Aging Cell* **13**, 121–130.
- Varol, C., Mildner, A., and Jung, S. (2015). Macrophages: development and tissue specialization. *Annu. Rev. Immunol.* **33**, 643–675.
- Wagenseil, J.E., and Mecham, R.P. (2009). Vascular extracellular matrix and arterial mechanics. *Physiol. Rev.* **89**, 957–989.
- Wagenseil, J.E., Nerurkar, N.L., Knutsen, R.H., Okamoto, R.J., Li, D.Y., and Mecham, R.P. (2005). Effects of elastin haploinsufficiency on the mechanical behavior of mouse arteries. *Am. J. Physiol. Heart Circ. Physiol.* **289**, H1209–H1217.
- Xu, H., Chen, M., Reid, D.M., and Forrester, J.V. (2007). LYVE-1-positive macrophages are present in normal murine eyes. *Invest. Ophthalmol. Vis. Sci.* **48**, 2162–2171.
- Yabluchanskiy, A., Ma, Y., Iyer, R.P., Hall, M.E., and Lindsey, M.L. (2013). Matrix metalloproteinase-9: Many shades of function in cardiovascular disease. *Physiology (Bethesda)* **28**, 391–403.
- Yu, Q., and Stamenkovic, I. (2000). Cell surface-localized matrix metalloproteinase-9 proteolytically activates TGF-beta and promotes tumor invasion and angiogenesis. *Genes Dev.* **14**, 163–176.

STAR★METHODS

KEY RESOURCES TABLE

REAGENT or RESOURCE	SOURCE	IDENTIFIER
Antibodies		
Anti-mouse CD45 (30-F11) BUV395	BD Horizon	Cat#564279; RRID: AB_2651134
Anti-mouse CD11b (M1/70) BV711	BioLegend	Cat#101241; RRID: AB_11218791
Anti-mouse CD64 (X54-5/7.1.1) PE	BD PharMingen	Cat#558455; RRID: AB_647241
Anti-mouse CD64 (X54-5/7.1) BV421	BioLegend	Cat#139309; RRID: AB_2562694
Anti-mouse Mer Biotinylated antibody	R&D Systems	Cat#BAF591; RRID: AB_2098563
Anti-mouse LYVE-1 (ALY7) eFluor660	eBioscience	Cat#50-0443-82; RRID: AB_10597449
Anti-mouse CD206 (MR5D3) PE	Bio-Rad	Cat#MCA2235PE; RRID: AB_324268
Anti-mouse MHCII (M5/114.15.2) BV510	BioLegend	Cat#107635; RRID: AB_2561397
Anti-mouse CD45 (30-F11) APC-Cy7	BD PharMingen	Cat#557659; RRID: AB_396774
Anti-mouse CD11b (M1/70) PerCP-Cy5.5	BD PharMingen	Cat#550993; RRID: AB_394002
Anti-mouse Ly6C (HK1.4) APC-Cy7	BioLegend	Cat#128026; RRID: AB_10640120
Anti-mouse F4/80 (BM8) eFluor450	eBioscience	Cat#48-4801-82; RRID: AB_1548747
Anti-mouse CD115 (AFS98) PE	Invitrogen	Cat#12-1152-82; RRID: AB_465808
Anti-mouse CD115 (AFS98) PE-Cy7	eBioscience	Cat#25-1152-82; RRID: AB_2573386
Anti-mouse Gr-1 (RB6-8C5) APC	BD PharMingen	Cat#553129; RRID: AB_398532
Anti-mouse CD44 (IM7) PE	eBioscience	Cat#12-0441-83; RRID: AB_465665
PE-CF594 Streptavidin	BD Horizon	Cat#562284; RRID: AB_11154598
Rabbit polyclonal LYVE-1	Abcam	Cat#Ab14917; RRID: AB_301509
Rat monoclonal CD68 (clone: FA-11)	Bio-rad	Cat#MCA1957; RRID: AB_322219
Rat monoclonal MHCII (I-A/I-E) (clone: M5/114.15.12)	eBioscience	Cat#14-5321-81; RRID: AB_467560
Goat polyclonal CD163	Santa Cruz	Cat#sc-18796; RRID: AB_2291274
Rat monoclonal CD206 (clone: MR5D3)	Bio-rad	Cat#MCA2235; RRID: AB_324622
Hamster monoclonal CD31 (clone: 2H8)	Millipore	Cat#MAB1398Z; RRID: AB_94207
Chicken polyclonal GFP	Aves Lab	Cat#GFP-1020; RRID: AB_10000240
Rabbit polyclonal Collagen type I	Millipore	Cat#AB765P; RRID: AB_92259
Rabbit polyclonal MMP-9	Abcam	Cat#ab38898; RRID: AB_776512
Rat Monoclonal LYVE-1 (clone: 223322)	R&D systems	Cat#MAB2125; RRID: AB_2138528
Goat polyclonal LYVE-1	R&D systems	Cat#AF2089; RRID: AB_355144
Mouse monoclonal CD31 (clone: WM59)	PharMingen	Cat#550389; RRID: AB_2252087
SMA (Cy3) (clone: 1A4)	Sigma-Aldrich	Cat#C6198; RRID: AB_476856
SMA (Cy2) (clone: 1A4)	Sigma-Aldrich	Cat#F3777; RRID: AB_476977
Anti-rat AF488 secondary	JacksonImmuno	Cat#712-545-153; RRID: AB_2340684
Anti-rat Cy3 secondary	JacksonImmuno	Cat#712-165-153; RRID: AB_2340667
Anti-rat AF647 secondary	JacksonImmuno	Cat#712-605-153; RRID: AB_2340694
Anti-rabbit AF488 secondary	JacksonImmuno	Cat#711-545-152; RRID: AB_2313584
Anti-rabbit Cy3 secondary	JacksonImmuno	Cat#711-165-152; RRID: AB_2307443
Anti-chicken AF488 secondary	JacksonImmuno	Cat#703-545-155; RRID: AB_2340375
Anti-Armenian hamster AF647 secondary	JacksonImmuno	Cat#127-605-160; RRID: AB_2339001
Anti-mouse Cy3 secondary	JacksonImmuno	Cat#715-165-151; RRID: AB_2315777
Anti-goat AF488 secondary	JacksonImmuno	Cat#705-545-147; RRID: AB_2336933
Anti-goat Cy3 secondary	JacksonImmuno	Cat#705-165-147; RRID: AB_2307351
Rat Monoclonal LYVE-1 (clone C1/8)	Laboratory of Dr David Jackson	(Johnson et al., 2017)

(Continued on next page)

Continued

REAGENT or RESOURCE	SOURCE	IDENTIFIER
Rat monoclonal IgG2a Isotype control	Invitrogen	Cat#16-4321-85; RRID: AB_470157
Rat monoclonal CD44 (clone KM201)	Abcam	Cat#ab25340; RRID: AB_470456
Anti-mouse/rat integrin β 1 (clone HM β 1-1)	BioLegend	Cat#102209; RRID: AB_312886
Streptavidin-Cy3	JacksonImmuno	Cat#016-600-084; RRID: AB_2341101
Biological Samples		
Human skin	Tan Tock Seng Hospital, Singapore	N/A
Human Umbilical cord	National University Hospital, Singapore	N/A
Chemicals, Peptides, and Recombinant Proteins		
Ki20227	GVK Biosciences	N/A
Fluorescein dextran (70,000 MW)	Invitrogen	Cat#D1823
CountBright Absolute counting beads	Life Technologies	Cat# C36950
MMP-9 inhibitor	Calbiochem	Cat#444278-500UG
Hyaluronidase	Sigma-Aldrich	Cat#H1136
Methylumbelliferone	Sigma-Aldrich	Cat#M1508
DQ-gelatin	Invitrogen	Cat#D12054
Biotinylated hyaluronic acid binding protein	Calbiochem	Cat#385911
Recombinant mouse MMP-9	R&D Systems	Cat#909-MM
p-aminophenylmercuric acetate	Sigma	Cat#A-9563
Critical Commercial Assays		
Picro Sirius Red Stain Kit	Abcam	Cat#Ab150681
Sircol Collagen Assay	Biocolor	Cat#S1000
RNeasy Micro Kit	QIAGEN	Cat#74004
Taqman reverse transcription kit	Applied Biosystem	Cat#N8080234
mirVana miRNA Isolation kit	Life Technologies	Cat#AM1560
Ovation PicoSL WTA System V2	NuGEN	Cat#3312-24
SYBR Green PCR Master Mix	Applied Biosystem	Cat#1725124
Arcturus PicoPure RNA Isolation kit	Applied Biosystem	Cat#KIT0204
ERCC RNA Spike in Controls	Ambion	Cat#4456740
Illumina Nextera XT kit	Illumina	Cat#FC-131-1024
DNA High Sensitivity Reagent Kit	Perkin Elmer	Cat#CLS760672
Deposited Data		
RNA seq of LYVE-1 ⁺ and LYVE-1 ⁻ mac from mouse aorta and adipose tissue	This paper	GEO: GSE114630
Experimental Models: Organisms/Strains		
Mouse: C57BL/6	Comparative Medicine, National University of Singapore	N/A
Mouse: MaFIA	SigN, Singapore	Burnett et al., 2004
Mouse: <i>Cx3cr1</i> ^{gfp/+}	SigN, Singapore	N/A
Mouse: <i>Mmp9</i> ^{-/-}	SigN, Singapore	N/A
Mouse: <i>Lyve1</i> ^{-/-} and <i>Lyve1</i> ^{+/+}	Laboratory of Dr David Jackson	Gale et al., 2007
Mouse: <i>Apoe</i> ^{-/-}	The Jackson Laboratory	Cat#002052
Mouse: <i>Lyve1</i> ^{cre/cre}	The Jackson Laboratory	Cat#012601
Mouse: <i>Csf1</i> ^{flox/flox}	The Jackson Laboratory	Cat#021212
Mouse: <i>Lyve1</i> ^{wt/cre} ; <i>Csf1</i> ^{flox/flox}	Bred in house	This paper

(Continued on next page)

Continued

REAGENT or RESOURCE	SOURCE	IDENTIFIER
Software and Algorithms		
Flowjo	Tree Star	https://www.flowjo.com/solutions/flowjo/downloads
Prism	Graphpad	https://www.graphpad.com
Imaris	Bitplane	http://www.bitplane.com/download
ImageJ	NIH	https://imagej.nih.gov/ij/download.html
R v3.3.0	R	https://www.r-project.org/
Bioconductor v3.3	Bioconductor	https://www.bioconductor.org/
STAR v2.5.2b	STAR	https://code.google.com/archive/p/rna-star/
GENCODE Release M7 (GRCm38.p4)	GENCODE	https://www.genecodegenes.org/
featureCounts v1.5.0	SUBREAD package	http://subread.sourceforge.net/
edgeR v3.14.0	Bioconductor	http://bioconductor.org/packages/release/bioc/html/edgeR.html
limma v3.28.14	Bioconductor	https://bioconductor.org/packages/release/bioc/html/limma.html

CONTACT FOR REAGENT AND RESOURCE SHARING

Further information and requests for resources and reagents should be directed to and will be fulfilled by the Lead Contact, Veronique Angeli (veronique_angeli@nuhs.edu.sg).

METHOD DETAILS**Mice**

C57BL/6 and albino C57BL/6 WT mice were purchased from Comparative Medicine (National University of Singapore). Macrophage Fas-Induced Apoptosis (MaFIA) mice were obtained from Florent Ginhoux ([Burnett et al., 2004](#)). *Cx3cr1^{gfp/+}* and *Mmp9^{-/-}* mice were obtained from Lai Guan Ng (SigN, Singapore). Tissues from *Lyve1^{-/-}* and *Lyve1^{+/+}* littermates were obtained from David Jackson ([Gale et al., 2007](#)). *Lyve1^{cre/cre}* and *Csf1^{flox/flox}* were purchased from Jackson Laboratory and cross breed to generate *Lyve1^{wt/cre};Csf1^{flox/flox}* mice. WT and *Apoe^{-/-}* were maintained on a high fat diet (21% fat and 0.15% cholesterol; Teklad) from 6 weeks of age. Animals of either sex (except for *Csf1^{flox/flox}* and *Lyve1^{wt/cre};Csf1^{flox/flox}* mice, in which only females were used) were euthanized at various ages ranging from 6-30 weeks of age for experiments. All animals were maintained in specific pathogen-free animal facility and were handled in accordance to protocols approved by the institutional animal care and use committees (IACUC) of the National University of Singapore and Singapore Immunology Network.

Human materials

Human skin was obtained from healthy subject under a Tang Tock Seng Hospital institutional review board-approved protocol after informed consent in accordance with the Declaration of Helsinki. Human umbilical cords were obtained after full term delivery of healthy infants from the National University Hospital and their use in this project was approved by the Ministry of Health Institutional Domain Specific Review Board (DSRB), Singapore after written informed patient consent.

Animal treatment

6 weeks old C57BL/6 WT mice received daily oral administration of Ki20227 (30mg/kg) or vehicle (0.05% methylcellulose) for 2, 14 or 24 weeks ([Kubota et al., 2009](#)). *Apoe^{-/-}* and matching WT mice around 9-10 weeks of age received daily oral administration of Ki20227 for 9 weeks. MaFIA mice were treated by daily intraperitoneal injection of 10mg/kg AP20187 or vehicle which consists of 0.05% methylcellulose ([Burnett et al., 2004](#)) for 4 consecutive days and sacrificed 15 days after last injection.

Transplantation of congenic bone marrow cells

Seven to eight weeks old CD45.2⁺ C57BL/6 recipient mice were lethally irradiated with two doses 480 rad each and 1 × 10⁶ CD45.1⁺ bone marrow cells were adoptively transfer via tail vein injection. To isolate bone marrow cells, CD45.1⁺ mouse femur and tibia were flushed with 27-gauge needles with DMEM supplemented with 2mM L-glutamine, 10% FBS, 4% HEPES and 1% Penicillin

and streptomycin. Cell suspension was filtered through 70 μm cell strainer (BD Falcon). Cells were pelleted by centrifugation and counted with Trypan blue exclusion method. Successful chimerism was confirmed by 100% non-host chimerism of blood monocytes after 1 month, as described previously by Hashimoto and coworker that all Gr1^{high} and Gr1^{low} monocytes in peripheral blood were replaced by donor cells after 2 weeks (Hashimoto et al., 2013).

Blood pressure measurements

Blood pressure was measured non-invasively on conscious mice using the tail cuff system (BP2000 system, Visitech Systems). Mice were placed in warmed restraining chambers and acclimatized to the experimental procedure for 4 days. Readings were recorded for 20 cycles and collected for the next 3 days. Data points for each mouse was averaged across last 3 days readings to determine systolic, diastolic and mean blood pressure.

Tissue processing, flow cytometry and cell sorting

Blood monocytes were collected by terminal cardiac puncture with 0.5M EDTA as anticoagulant. Epididymal and subcutaneous fats were extracted, minced and digested with 25 $\mu\text{g}/\text{ml}$ LiberaseTM Research Grade (Roche) for 1 hour with shaking at 37°C. Aorta and ear skin were extracted, minced and digested for 2 hours with 1mg/ml and 2mg/ml Collagenase Type IV (GIBCO) respectively. The digested materials were filtered through 160 μm nylon mesh filter and pelleted by centrifugation (1000 g, 10 minutes for adipose tissues, and 1200rpm, 5 minutes for aorta and ears) at 4°C. Red blood cells were lysed with 0.9% ammonium chloride and then resuspended with FACS buffer (PBS containing 0.5% FBS and 2mM EDTA). For aorta samples, two aortas were pooled into one point to get sufficient cell numbers with the exception of aortic adventitia and intima-media analysis whereby 10 aortas were pooled for one data point. Cells were stained at 4°C in FACS buffer containing 1% normal mouse serum (Jackson ImmunoResearch Laboratories). Fluorochrome- and biotin-conjugated antibodies specific to mouse CD45 (clone 30-F11), CD11b (clone M1/70), LYVE-1 (clone ALY7), CD115 (clone AFS98), CD206 (clone MR5D3), F4/80 (clone BM8), CD64 (clone X54-5/7.1.1), MerTK (R&D System), MHCII (clone M5/114.15.2), Ly6C (clone HK1.4) and streptavidin PE-CF594 (BD Horizon) were used. Macrophages were identified as CD45⁺ CD11b⁺ CD64⁺ MerTK⁺ F4/80⁺ MHCII^{+/-}. Blood monocytes were identified as CD45⁺ CD11b⁺ F4/80^{low} CD115⁺ Ly6C^{low/high}. Aortic monocytes were identified as CD45⁺ CD11b⁺ Ly6C⁺. DAPI were used to exclude the dead cells. CountBrightTM Absolute counting beads (Life Technologies) was used for quantification of cell numbers. The cells were acquired on LSR Fortessa X-20 (BD Biosciences) and analyzed with Flowjo Software (Tree Star, Inc). For cell sorting, the procedures were performed with Sy3200 Cell Sorter (Sony Biotechnology Inc.). LYVE-1⁺ and LYVE-1⁻ macrophages were identified and sorted as CD45⁺ CD11b⁺ CD206⁺ LYVE-1⁺ and CD45⁺ CD11b⁺ CD206⁻ LYVE-1⁻ respectively with > 98% purity. This was further confirmed by gene expression analysis of *Lyve1* by RT-PCR in sorted cells (data not shown).

Immunohistochemistry

Cryo-sections from mouse skin (10 μm), aorta (7 μm), brain (10 μm), adipose tissues (10 μm), esophagus (10 μm), human skin (80 μm) and human umbilical cord (12 μm) were prepared for immunohistochemistry. Acetone-fixed sections were used for most immunostaining whereas 2% paraformaldehyde (PFA) + 30% sucrose fixative was used for fluorescent-tagged transgenic mice samples and human skin samples. Primary antibodies used for mouse tissues included anti-LYVE-1 (rabbit polyclonal; Abcam), anti-CD68 (rat clone FA-11; Bio-rad), anti-MHCII (rat clone M5/114.15.2; eBioscience), anti-CD163 (goat polyclonal; Santa Cruz), anti-CD206 (rat clone MR5D3; Bio-rad), anti-CD31 (armenian hamster clone 2H8; Chemicon), anti-GFP (chicken polyclonal; Aves Lab), anti-collagen type I (rabbit polyclonal; Millipore), anti-MMP-9 (rabbit polyclonal; Abcam) and anti-LYVE-1 (rat clone 223322; R&D Systems). Primary antibodies used for human skin samples include anti-LYVE-1 (goat polyclonal, R&D Systems) and anti-CD31 (mouse clone WM59; PharMingen). For isotype controls, biotinylated rat (eBioscience), biotinylated mouse IgG (PharMingen) rat IgG (eBioscience), armenian hamster IgG (eBioscience), rabbit and goat IgG (Jackson Immunoresearch) were used. AF488-, Cy3- and AF647- conjugated antibodies from Jackson Immunoresearch were used for detection. FITC or Cy3-conjugated anti smooth muscle actin (SMA, mouse clone 1A4; Sigma-Aldrich) was used to identify smooth muscle cells. Sections were counterstained with 4,6-diamidino-2-phenylindole (DAPI) for cell nuclei visualization and mounted for analysis.

Ear skin, trachea, brain meninges and aorta were processed for whole mount staining. Mice were perfused with 2% PFA, and the tissue was removed and placed into the fixative overnight at 4°C. Tissues were rinsed several with PBS followed by splitting of the ears into dorsal and ventral halves. The samples were blocked with PBS containing 0.5% bovine serum albumin and 0.3% Triton overnight at 4°C, incubated overnight at 4°C with primary antibodies against LYVE-1, CD31, CD68, CD206, MHCII, SMA and GFP for fluorescent-tagged mouse ears and aortas. The tissues were then washed and stained overnight with fluorescent (AF488, AF647 and Cy3) secondary antibodies (Jackson Immunoresearch). For colorimetric detection, whole mount aortas were first incubated with 3% hydrogen peroxide for 30 mins to remove endogenous horseradish peroxidase (HRP) before blocking and primary rabbit anti-LYVE-1 staining. Aorta samples were then incubated with HRP-conjugated rabbit secondary antibody (Jackson Immunoresearch) followed by the substrate diaminobenzidine (DAB; Vector laboratories) to reveal staining. Picrosirius (Abcam) staining was performed using a commercially available kit as according to manufacturer instructions.

Specimens were viewed with a fluorescence widefield (Axio Imager.Z1, AxioCam HRM camera; Carl Zeiss Micro Imaging, Inc., Jena, Germany) or confocal microscope (Leica TCS SP5; Leica Microsystems, Inc., Deerfield, IL) using LAS AF confocal software (version 1.8.2; Leica Microsystems, Inc). For multi-photon imaging of mouse ears, a TriM Scope II single-beam two-photon microscope (LaVision BioTec) with a tunable 680-1080nm laser (Coherent) was used to acquire the images. AF488, AF647, Cy3 and second harmonic generation (SHG; collagen in ear dermis) were simultaneously excited at 800nm (or at 950nm without AF647), and emitted light was detected through 655/40nm, 579/34nm, 525/50nm and 390/40nm or 475/42nm filters respectively. 100-120 μ m z stacks were obtained at intervals of 2 μ m. Imaris software (Bitplane) was used to analyze the images obtained.

For SMCs immunostaining, cells were fixed with 2% paraformaldehyde (PFA) for 10 minutes. Cells were first incubated with an avidin and biotin blocking kit (Vector laboratories) to block endogenous biotin before staining with primary antibody against Collagen Type I (Millipore), Cy3-conjugated SMA (Sigma) and biotinylated HA-BP (Calbiochem) overnight at 4°C, followed by AF488 and AF647-conjugated secondary antibody (Jackson ImmunoResearch) at room temperature for 1.5 hours. Subsequent microscopy procedures were carried out as described above.

In vivo and in vitro phagocytosis assay

C57BL/6 WT mice received subcutaneous injections of 70kD fluorescent FITC-dextran into the ear and front footpad skin 24 hours before euthanization and was processed for subsequent immunofluorescence microscopy. *In vitro* phagocytosis was done by incubating the aorta and skin cell suspensions with 70kD fluorescent FITC-dextran (0.5 mg/ml) for 45 minutes at 4°C and 37°C prior analysis by flow cytometry.

Vascular smooth muscle cells culture and assays

Primary mouse vascular smooth muscle cells were isolated from thoracic aorta of 6-8 weeks old C57BL/6 WT mice of either sex. The cells were prepared by explant methods as previously described (Kothapalli et al., 2012). Briefly, thoracic aorta with fats removed was cut open and intimal layer was scraped off. The aorta was cut into smaller pieces and SMCs were allowed to grow out from the explants for 7-10 days in growth medium (1:1 DMEM/F12 supplemented with 2 mM L-glutamine and 20% FBS). The passage 1-2 SMCs were used in the experiments and their identity was confirmed by α -SMA staining. For the co-culture experiments, LYVE-1⁺ and LYVE-1⁻ macrophages were isolated from epididymal and subcutaneous adipose tissues followed by cell sorting as described above. The viability of LYVE-1⁺ and LYVE-1⁻ macrophages was > 83% both before and after 24 hours of culture. Co-cultures of LYVE-1⁺ macrophages and LYVE-1⁻ macrophages with SMCs were done in a 5:1 ratio. For the experiment with MMP-9 inhibitor, SMCs were pre-incubated with 5 μ M MMP-9 inhibitor (Calbiochem) 2 hours before the addition of LYVE-1⁺ macrophages. Subsequently 5 μ M MMP-9 inhibitor was added into the co-culture of SMCs with LYVE-1⁺ macrophages. For transwell experiment, LYVE-1⁺ macrophages were separated from SMCs via a transwell insert with 5 μ m pore size (Corning) for 24 hours. For the treatment of SMCs with MMP-9, activated-MMP-9 was generated by incubating pro-MMP-9 (R&D Systems) with p-aminophenylmercuric acetate (Sigma) for 2 hours at 37°C and the activation status of MMP-9 was further verified by western blot analysis (data not shown). SMCs were subsequently treated with 50ng/ml and 100ng/ml of pro-MMP-9 or activated MMP-9 for 24 hours. CD44 and integrin β 1 blocking experiment was carried out by pre-incubating LYVE-1⁺ macrophages with 10 μ g/ml anti-CD44 (abcam) or 10 μ g/ml anti-integrin β 1 antibodies (BioLegend) for 30 minutes prior to addition into SMCs for 24 hours. LYVE-1 blocking antibodies (mAb 2125 and C1/8) were provided by David Jackson (Weatherall Institute of Molecular Medicine, Oxford, UK). LYVE-1 blocking experiments were carried out by pre-incubating LYVE-1⁺ macrophages with 50 μ g/ml of anti-LYVE-1 antibody and Rat IgG2a (eBioscience) for 30 minutes before co-culture with SMCs for 24 hours. For the co-culture experiment with hyaluronidase, SMCs were treated with 5U/ml hyaluronidase (Sigma) for 2 hours before the addition of 4-Methylumbelliferone (Sigma) and LYVE-1⁺ macrophages for 24 hours. All the experiments were done on 8-well chamber slides (ibidi).

In situ gelatin zymography for in vivo studies

A quenched fluorescein-labeled gelatinase substrate, DQ-gelatin (Invitrogen) was used to detect gelatinolytic activity. The resultant fluorescence signal reflects the extent of proteolytic digestion by gelatinases (MMP-9 and MMP-2). Fresh tissue sections were incubated with 1% low melting temperature (LMT) agarose (Promega) containing DQ-gelatin (0.1mg/ml) for 3 hours at room temperature. Tissue sections pretreated with Protease K inhibitor for 5 mins (2 μ g/ml; Promega) and sections incubated with agarose gel lacking DQ-gelatin served as negative control (data not shown). DQ-gelatin signals were view under a fluorescence microscope using a filter set with excitation of 480 nm.

Data analysis and quantification

No human samples or animals were excluded from any analyses. For animal studies, samples were not randomized to experimental groups and animal numbers were empirically determined to optimize numbers necessary based on our previous studies or pilot experiments. All analyses were performed unblinded except for quantification of numbers of LYVE-1⁺ macrophages and assessment of arterial wall remodeling in mice.

For quantification of LYVE-1⁺ macrophages number in aorta sections, colocalization of macrophage pan-marker CD68 was used to identify and count LYVE-1⁺ macrophages.

Adventitial area, medial diameter and thickness were quantified using 5 mm of the descending aorta near the renal artery. Medial diameter was calculated based on the circumference of the inner elastin laminae. GFP autofluorescence of elastin lamellae enable clear demarcation of the inner (IEL) and external elastic laminae (EEL) regions. Adventitial area was measured by using collagen type I staining and GFP autofluorescence of EEL to define medial-adventitial border. Distance of CD68⁺ macrophages were measured from the center of the cell to the external elastic laminae (EEL).

For the quantification of collagen type I, each SMC was outlined based on the staining with α -SMA and the fluorescence intensity of collagen was measured. At least 60 cells were scored in two independent experiments. Fluorescence intensity of all treatment groups were normalized to non-treated group. All quantitative histological images were processed using ImageJ (NIH, Bethesda).

Circumference tensile and contractility tests

These tests were performed according to previously established protocols with some minor modifications (Tan et al., 2013). Briefly, the descending abdominal aorta was isolated and denuded of periaortic tissues and blood. Aortic segments were subsequently mounted onto a small vessel myograph (model 410A; Danish Myotechnology) and submerged in Krebs-Henseleit Buffer at 37°C. The segments were then stretched at a steady increment of 50 μ m per min until breakage. The wall stress was calculated by dividing the force generated with the surface area of the aortic segment. The corresponding strain was calculated by measuring the net distance stretched (ΔL) over original distance between the two wires (L_0). The stress-strain curve was then fitted on an exponential curve. Stiffness of the aorta was determined by the gradient of the stress-strain curve. For contractility test, aortic segments were stretched to a tension of 1 g. The vessels were then challenged with 80 mmol/L KCl and the maximal contractile force was recorded.

RNA-seq, differential gene expression, and functional enrichment analyses

Total RNA was extracted using Arcturus PicoPure RNA Isolation kit (Applied Biosystems Thermo Fisher Scientific) according to manufacturer's protocol. All mouse RNAs were analyzed on Agilent Bioanalyser for quality assessment with RNA Integrity Number (RIN) range from 7.7 to 9.1 and median RIN 8.3. cDNA libraries were prepared using 2 ng of total RNA and 1 μ l of a 1:50,000 dilution of ERCC RNA Spike in Controls (Ambion® Thermo Fisher Scientific) using the SMARTSeq v2 protocol with the following modifications: 1. Addition of 20 μ M TSO; 2. Use of 250 pg cDNA with 1/5 reaction of Illumina Nextera XT kit (Illumina, San Diego, CA, USA). The length distribution of the cDNA libraries was monitored using a DNA High Sensitivity Reagent Kit on the Perkin Elmer Labchip (Perkin Elmer, Waltham, MA, USA). 12 samples were subjected to an indexed PE sequencing run of 2x51 cycles on an Illumina HiSeq 2000 (20 samples/lane) and 1 sample was subjected to an indexed PE sequencing run of 2x51 cycles on an Illumina HiSeq 2500 Rapid mode (14 samples/lane).

Unaligned reads in fastq files obtained by RNA-Seq were mapped to the mouse genome built mm10, with a junction database based on Gencode GRCm38 (release M7), using the STAR alignment software version 2.5.2b. The general-purpose read summarization function featureCounts v1.5.0 was then used to assign mapped reads to genes.

The differential gene expression analysis between LYVE-1⁺ and LYVE-1⁻ macrophages in the fat tissue followed the limma-voom (v3.28.14) protocol. Raw counts obtained with featureCounts were TMM-normalized and voom-transformed [$\log_2(\text{Counts Per Million})$], and limma's empirical Bayes moderated t tests were applied to detect differentially expressed genes, adjusting the resulting p values for multiple testing by the Benjamini-Hochberg method. An adjusted p value of 0.05 used as threshold yielded 243 differentially expressed genes, further stratified, according to the sign of their logFC (log fold change) value, into 85 and 158 genes upregulated and downregulated, respectively, in LYVE-1⁺ macrophages.

Hypergeometric tests were performed on lists of genes upregulated and downregulated in LYVE-1⁺ macrophages, in order to detect significant enrichment of biological processes in the Gene Ontology (GO); p values were corrected using the Benjamini-Hochberg method, and a threshold of 0.05 was applied. Analyses were performed in R v 3.3.0/bioconductor.

Quantitative real-time PCR

Dissected mouse aortas were infused with an RNA stabilizing reagent (RNA later, QIAGEN) for an hour at 4 degrees. The aortic adventitia layer was carefully separated from the media and intima layer and kept in Trizol reagent for tissue homogenization. Total mRNA was isolated from mouse tissues using an mRNA isolation kit (RNeasy Micro Kit, QIAGEN) according to the manufacturer's instructions. cDNA was synthesized from 500ng of RNA using Taqman reverse transcription kit (Applied Biosystems).

For sorted LYVE-1⁺ and LYVE-1⁻ macrophages, the cells were kept in Lysis-Binding buffer provided in mirVanaTM miRNA Isolation Kit (Life Technologies). Total mRNA was isolated from cells using the mirVanaTM miRNA Isolation Kit according to the manufacturer's instructions. cDNA was amplified and synthesized using Ovation PicoSL WTA System V2 (NuGEN) according to the manufacturer's instructions.

Real time quantitative PCR was performed in triplicates using SYBR Green PCR Master Mix (Applied Biosystems) and analyzed on an Abi Prism 7500 Detection System (Applied Biosystems, Warrington, UK). Data was normalized with r12S and primers are listed below.

GENE	Forward primer 5'-3'	Reverse Primer 5'-3'
<i>R12s</i>	GGAAGGCATAGTGTGGAGGT	CGATGACATCCTTGGCCTGA
<i>Lyve1</i>	TGGTGTACTCCTCGCCTCT	TTCTGCGCTGACTCTACCTG
<i>Csf1</i>	CCCATATTGCGACACCGAA	AAGCAGTAACTGAGCAACGGG
<i>Csf1r</i>	CCCCGTGCCAGCCGACTCTC	GGCCATCCCATTCCACACTGC
<i>Eln</i>	CGGGTCTGACAGCGGTAGT	CTCCAAGTCCTCCAGGACCT
<i>Col1a1</i>	ATGTTTCAGCTTTGTGGACCT	CAGCTGACTTCAGGGATGT
<i>Col3a1</i>	ATACCCGGAACACGAGGTC	CATCTTCGCCCTTAGGTCTCG
<i>Fibronectin</i>	TCATCCCAGAGGTGCCCAACTC	GTCCACCTCAGGCCGATGCTTG
<i>Mmp2</i>	TTCAGGTAATAAGCACCTTGAA	TAACCTGGATGCCGTCGT
<i>Mmp3</i>	GATCTCTTCATTTTGGCCATCTTTC	CTCCAGTATTTGCCTCTACAAAGAA
<i>Mmp9</i>	CGGCACGCCTTGGTGTAGCA	AGGTGAGGGGGCGCCTGTAG
<i>Timp1</i>	TCCCCAGAAATCAACGAGACCAC	AGAGTACGCCAGGGAACCAAGAAG
<i>Timp2</i>	CTACACGGCCCCCTTTCAGCAGT	CAAGGGATCATGGGACAGCGAGTG
<i>Timp3</i>	CAGGGCGCGTGTATGAAGG	CCGGATGCAGGCGTAGTG

QUANTIFICATION AND STATISTICAL ANALYSIS

Statistical analysis was performed with Graphpad Prism version 5.0 (GraphPad Software) Data were presented as mean \pm SEM and were analyzed by nonparametric Mann-Whitney U and Kruskal-Wallis tests for comparison between 2 groups and multiple groups (≥ 3), respectively for *in vivo* work. For *in vitro* studies, one-way ANOVA was used for multiple group comparisons. A *p* value of less than 0.05 was considered to be statistically significant.

DATA AND SOFTWARE AVAILABILITY

The RNaseq data discussed in this publication have been deposited in NCBI's Gene Expression Omnibus (Edgar et al., 2002) and are accessible through GEO Series accession number GSE114630 (<https://www.ncbi.nlm.nih.gov/geo/query/acc.cgi?acc=GSE114630>).